

1

Interactions of particles and radiation with matter

When the intervals, passages, connections, weights, impulses, collisions, movement, order, and position of the atoms interchange, so also must the things formed by them change.

Lucretius

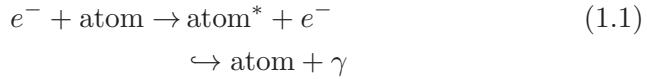
Particles and radiation can be detected only through their interactions with matter. There are specific interactions for charged particles which are different from those of neutral particles, e.g. of photons. One can say that every interaction process can be used as a basis for a detector concept. The variety of these processes is quite rich and, as a consequence, a large number of detection devices for particles and radiation exist. In addition, for one and the same particle, different interaction processes at different energies may be relevant.

In this chapter, the main interaction mechanisms will be presented in a comprehensive fashion. Special effects will be dealt with when the individual detectors are being presented. The interaction processes and their cross sections will not be derived from basic principles but are presented only in their results, as they are used for particle detectors.

The main interactions of charged particles with matter are *ionisation* and *excitation*. For relativistic particles, *bremssstrahlung* energy losses must also be considered. Neutral particles must produce charged particles in an interaction that are then detected via their characteristic interaction processes. In the case of photons, these processes are the photoelectric effect, Compton scattering and pair production of electrons. The electrons produced in these *photon interactions* can be observed through their ionisation in the sensitive volume of the detector.

1.1 Interactions of charged particles

Charged particles passing through matter lose kinetic energy by *excitation* of bound electrons and by *ionisation*. Excitation processes like



lead to low-energy photons and are therefore useful for particle detectors which can record this luminescence. Of greater importance are pure scattering processes in which incident particles transfer a certain amount of their energy to atomic electrons so that they are liberated from the atom.

The *maximum transferable kinetic energy* to an electron depends on the mass m_0 and the momentum of the incident particle. Given the momentum of the incident particle

$$p = \gamma m_0 \beta c, \quad (1.2)$$

where γ is the Lorentz factor ($= E/m_0 c^2$), $\beta c = v$ the velocity, and m_0 the rest mass, the maximum energy that may be transferred to an electron (mass m_e) is given by [1] (see also Problem 1.6)

$$E_{\text{kin}}^{\text{max}} = \frac{2m_e c^2 \beta^2 \gamma^2}{1 + 2\gamma m_e/m_0 + (m_e/m_0)^2} = \frac{2m_e p^2}{m_0^2 + m_e^2 + 2m_e E/c^2}. \quad (1.3)$$

In this case, it makes sense to give the kinetic energy, rather than total energy, since the electron is already there and does not have to be produced. The kinetic energy E_{kin} is related to the total energy E according to

$$E_{\text{kin}} = E - m_0 c^2 = c \sqrt{p^2 + m_0^2 c^2} - m_0 c^2. \quad (1.4)$$

For low energies

$$2\gamma m_e/m_0 \ll 1 \quad (1.5)$$

and under the assumption that the incident particles are heavier than electrons ($m_0 > m_e$) Eq. (1.3) can be approximated by

$$E_{\text{kin}}^{\text{max}} \approx 2m_e c^2 \beta^2 \gamma^2. \quad (1.6)$$

A particle (e.g. a muon, $m_\mu c^2 = 106 \text{ MeV}$) with a Lorentz factor of $\gamma = E/m_0 c^2 = 10$ corresponding to $E = 1.06 \text{ GeV}$ can transfer approximately 100 MeV to an electron (mass $m_e c^2 = 0.511 \text{ MeV}$).

If one neglects the quadratic term in the denominator of Eq. (1.3), $(m_e/m_0)^2 \ll 1$, which is a good assumption for all incident particles except for electrons, it follows that

$$E_{\text{kin}}^{\text{max}} = \frac{p^2}{\gamma m_0 + m_0^2/2m_e} . \quad (1.7)$$

For relativistic particles $E_{\text{kin}} \approx E$ and $pc \approx E$ holds. Consequently, the maximum transferable energy is

$$E^{\text{max}} \approx \frac{E^2}{E + m_0^2 c^2 / 2m_e} \quad (1.8)$$

which for muons gives

$$E^{\text{max}} = \frac{E^2}{E + 11 \text{ GeV}} . \quad (1.9)$$

In the extreme relativistic case ($E \gg m_0^2 c^2 / 2m_e$), the total energy can be transferred to the electron.

If the incident particle is an electron, these approximations are no longer valid. In this case, one gets, compare Eq. (1.3),

$$E_{\text{kin}}^{\text{max}} = \frac{p^2}{m_e + E/c^2} = \frac{E^2 - m_e^2 c^4}{E + m_e c^2} = E - m_e c^2 , \quad (1.10)$$

which is also expected in classical non-relativistic kinematics for particles of equal mass for a central collision.

1.1.1 Energy loss by ionisation and excitation

The treatment of the maximum transferable energy has already shown that incident electrons, in contrast to heavy particles ($m_0 \gg m_e$), play a special rôle. Therefore, to begin with, we give the energy loss for ‘heavy’ particles. Following Bethe and Bloch [2–8]*, the average energy loss dE per length dx is given by

$$-\frac{dE}{dx} = 4\pi N_A r_e^2 m_e c^2 z^2 \frac{Z}{A} \frac{1}{\beta^2} \left(\ln \frac{2m_e c^2 \gamma^2 \beta^2}{I} - \beta^2 - \frac{\delta}{2} \right) , \quad (1.11)$$

* For the following considerations and formulae, not only the original literature but also secondary literature was used, mainly [1, 4–12] and references therein.

where

z – charge of the incident particle in units of the elementary charge

Z, A – atomic number and atomic weight of the absorber

m_e – electron mass

r_e – classical electron radius ($r_e = \frac{1}{4\pi\epsilon_0} \cdot \frac{e^2}{m_e c^2}$ with ϵ_0 – permittivity of free space)

N_A – Avogadro number (= number of atoms per gram atom) = $6.022 \cdot 10^{23} \text{ mol}^{-1}$

I – mean excitation energy, characteristic of the absorber material, which can be approximated by

$$I = 16 Z^{0.9} \text{ eV} \quad \text{for } Z > 1 .$$

To a certain extent, I also depends on the molecular state of the absorber atoms, e.g. $I = 15 \text{ eV}$ for atomic and 19.2 eV for molecular hydrogen. For liquid hydrogen, I is 21.8 eV .

δ – is a parameter which describes how much the extended transverse electric field of incident relativistic particles is screened by the charge density of the atomic electrons. In this way, the energy loss is reduced (*density effect*, ‘Fermi plateau’ of the energy loss). As already indicated by the name, this density effect is important in dense absorber materials. For gases under normal pressure and for not too high energies, it can be neglected.

For energetic particles, δ can be approximated by

$$\delta = 2 \ln \gamma + \zeta ,$$

where ζ is a material-dependent constant.

Various approximations for δ and material dependences for parameters, which describe the density effect, are discussed extensively in the literature [9]. At very high energies

$$\delta/2 = \ln(\hbar\omega_p/I) + \ln \beta\gamma - 1/2 ,$$

where $\hbar\omega_p = \sqrt{4\pi N_e r_e^3 m_e c^2 / \alpha} = 28.8 \sqrt{\rho \langle Z/A \rangle} \text{ eV}$ is the plasma energy (ρ in g/cm^3), N_e the electron density, and α the fine-structure constant.

A useful constant appearing in Eq. (1.11) is

$$4\pi N_A r_e^2 m_e c^2 = 0.3071 \frac{\text{MeV}}{\text{g/cm}^2} . \quad (1.12)$$

In the logarithmic term of Eq. (1.11), the quantity $2m_e c^2 \gamma^2 \beta^2$ occurs in the numerator, which, according to Eq. (1.6), is identical to the maximum transferable energy. The average energy of electrons produced in the ionisation process in gases equals approximately the ionisation energy [2, 3].

If one uses the approximation for the maximum transferable energy, Eq. (1.6), and the shorthand

$$\kappa = 2\pi N_A r_e^2 m_e c^2 z^2 \cdot \frac{Z}{A} \cdot \frac{1}{\beta^2} , \quad (1.13)$$

the *Bethe–Bloch formula* can be written as

$$-\frac{dE}{dx} = 2\kappa \left(\ln \frac{E_{\text{kin}}^{\text{max}}}{I} - \beta^2 - \frac{\delta}{2} \right) . \quad (1.14)$$

The energy loss $-dE/dx$ is usually given in units of MeV/(g/cm²). The length unit dx (in g/cm²) is commonly used, because the energy loss per area density

$$dx = \varrho \cdot ds \quad (1.15)$$

with ϱ density (in g/cm³) and ds length (in cm) is largely independent of the properties of the material. This length unit dx consequently gives the area density of the material.

Equation (1.11) represents only an approximation for the energy loss of charged particles by ionisation and excitation in matter which is, however, precise at the level of a few per cent up to energies of several hundred GeV. However, Eq. (1.11) cannot be used for slow particles, i.e., for particles which move with velocities which are comparable to those of atomic electrons or slower. For these velocities ($\alpha z \gg \beta \geq 10^{-3}$, $\alpha = \frac{e^2}{4\pi\epsilon_0\hbar c}$: fine-structure constant) the energy loss is proportional to β . The energy loss of slow protons, e.g. in silicon, can be described by [10–12]

$$-\frac{dE}{dx} = 61.2 \beta \frac{\text{GeV}}{\text{g/cm}^2} , \quad \beta < 5 \cdot 10^{-3} . \quad (1.16)$$

Equation (1.11) is valid for all velocities

$$\beta \gg \alpha z . \quad (1.17)$$

Table 1.1. Average energy loss of minimum-ionising particles in various materials [10–12]; gases for standard pressure and temperature

Absorber	$\frac{dE}{dx} \Big _{\min} \left[\frac{\text{MeV}}{\text{g/cm}^2} \right]$	$\frac{dE}{dx} \Big _{\min} \left[\frac{\text{MeV}}{\text{cm}} \right]$
Hydrogen (H ₂)	4.10	$0.37 \cdot 10^{-3}$
Helium	1.94	$0.35 \cdot 10^{-3}$
Lithium	1.64	0.87
Beryllium	1.59	2.94
Carbon (Graphite)	1.75	3.96
Nitrogen	1.82	$2.28 \cdot 10^{-3}$
Oxygen	1.80	$2.57 \cdot 10^{-3}$
Air	1.82	$2.35 \cdot 10^{-3}$
Carbon dioxide	1.82	$3.60 \cdot 10^{-3}$
Neon	1.73	$1.56 \cdot 10^{-3}$
Aluminium	1.62	4.37
Silicon	1.66	3.87
Argon	1.52	$2.71 \cdot 10^{-3}$
Titanium	1.48	6.72
Iron	1.45	11.41
Copper	1.40	12.54
Germanium	1.37	7.29
Tin	1.26	9.21
Xenon	1.25	$7.32 \cdot 10^{-3}$
Tungsten	1.15	22.20
Platinum	1.13	24.24
Lead	1.13	12.83
Uranium	1.09	20.66
Water	1.99	1.99
Lucite	1.95	2.30
Shielding concrete	1.70	4.25
Quartz (SiO ₂)	1.70	3.74

Given this condition, the energy loss decreases like $1/\beta^2$ in the low-energy domain and reaches a broad minimum of ionisation near $\beta\gamma \approx 4$. Relativistic particles ($\beta \approx 1$), which have an energy loss corresponding to this minimum, are called *minimum-ionising particles* (MIPs). In light absorber materials, where the ratio $Z/A \approx 0.5$, the energy loss of minimum-ionising particles can be roughly represented by

$$-\frac{dE}{dx} \Big|_{\min} \approx 2 \frac{\text{MeV}}{\text{g/cm}^2} . \quad (1.18)$$

In Table 1.1, the energy losses of minimum-ionising particles in different materials are given; for further values, see [10–12].

The energy loss increases again for $\gamma > 4$ (*logarithmic rise* or *relativistic rise*) because of the logarithmic term in the bracket of Eq. (1.11). The increase follows approximately a dependence like $2 \ln \gamma$.

The decrease of the energy loss at the ionisation minimum with increasing atomic number of the absorber originates mainly from the Z/A term in Eq. (1.11). A large fraction of the logarithmic rise relates to large energy transfers to few electrons in the medium (δ rays or knock-on electrons). Because of the density effect, the logarithmic rise of the energy loss saturates at high energies.

For heavy projectiles (e.g. like copper nuclei), the energy loss of slow particles is modified because, while being slowed down, electrons get attached to the incident nuclei, thereby decreasing their effective charge.

The energy loss by ionisation and excitation for muons in iron is shown in Fig. 1.1 [10, 11, 13].

The energy loss according to Eq. (1.11) describes only energy losses due to ionisation and excitation. At high energies, radiation losses become more and more important (see Sect. 1.1.5).

Figure 1.2 shows the ionisation energy loss for electrons, muons, pions, protons, deuterons and α particles in air [14].

Equation (1.11) gives only the average energy loss of charged particles by ionisation and excitation. For thin absorbers (in the sense of Eq. (1.15), average energy loss $\langle \Delta E \rangle \ll E_{\max}$), in particular, strong fluctuations around the average energy loss exist. The energy-loss distribution for thin absorbers is strongly asymmetric [2, 3].

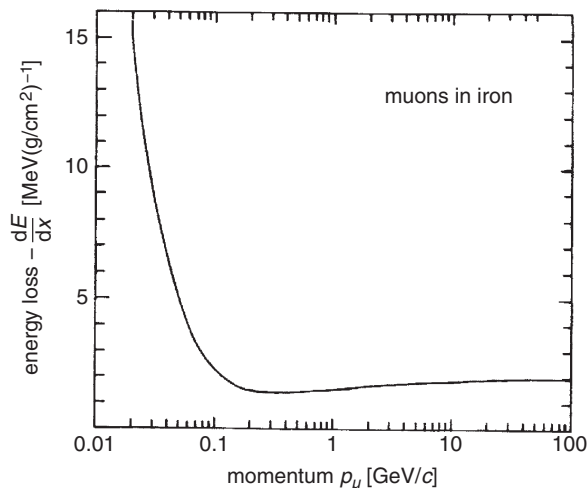


Fig. 1.1. Energy loss by ionisation and excitation for muons in iron and its dependence on the muon momentum.

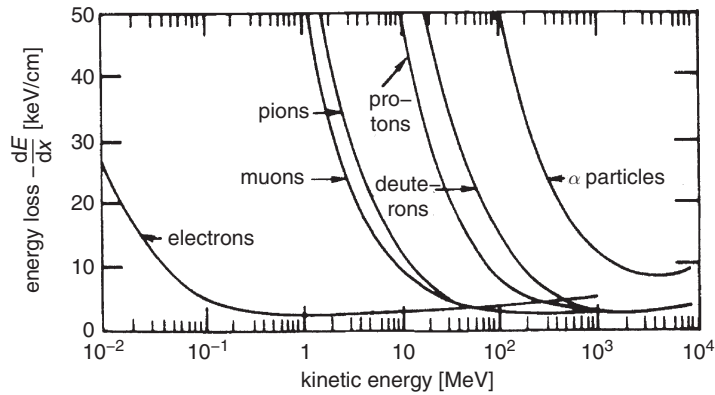


Fig. 1.2. Energy loss for electrons, muons, pions, protons, deuterons and α particles in air [14].

This behaviour can be parametrised by a *Landau distribution*. The Landau distribution is described by the inverse Laplace transform of the function s^s [15–18]. A reasonable approximation of the Landau distribution is given by [19–21]

$$L(\lambda) = \frac{1}{\sqrt{2\pi}} \cdot \exp \left[-\frac{1}{2}(\lambda + e^{-\lambda}) \right], \quad (1.19)$$

where λ characterises the deviation from the *most probable energy loss*,

$$\lambda = \frac{\Delta E - \Delta E^W}{\xi}, \quad (1.20)$$

ΔE – actual energy loss in a layer of thickness x ,

ΔE^W – most probable energy loss in a layer of thickness x ,

$$\xi = 2\pi N_A r_e^2 m_e c^2 z^2 \frac{Z}{A} \cdot \frac{1}{\beta^2} \rho x = \kappa \rho x \quad (1.21)$$

(ρ – density in g/cm^3 , x – absorber thickness in cm).

The general formula for the most probable energy loss is [12]

$$\Delta E^W = \xi \left[\ln \left(\frac{2m_e c^2 \gamma^2 \beta^2}{I} \right) + \ln \frac{\xi}{I} + 0.2 - \beta^2 - \delta(\beta\gamma) \right]. \quad (1.22)$$

For example, for argon and electrons of energies up to 3.54 MeV from a ^{106}Rh source the most probable energy loss is [19]

$$\Delta E^{\text{W}} = \xi \left[\ln \left(\frac{2m_e c^2 \gamma^2 \beta^2}{I^2} \xi \right) - \beta^2 + 0.423 \right]. \quad (1.23)$$

The most probable energy loss for minimum-ionising particles ($\beta\gamma = 4$) in 1 cm argon is $\Delta E^{\text{W}} = 1.2$ keV, which is significantly smaller than the average energy loss of 2.71 keV [2, 3, 19, 22]. Figure 1.3 shows the energy-loss distribution of 3 GeV electrons in a thin-gap drift chamber filled with Ar/CH₄ (80:20) [23].

Experimentally, one finds that the actual energy-loss distribution is frequently broader than represented by the Landau distribution.

For thick absorber layers, the tail of the Landau distribution originating from high energy transfers, however, is reduced [24]. For very thick absorbers ($\frac{dE}{dx} \cdot x \gg 2m_e c^2 \beta^2 \gamma^2$), the energy-loss distribution can be approximated by a Gaussian distribution.

The energy loss dE/dx in a compound of various elements i is given by

$$\frac{dE}{dx} \approx \sum_i f_i \left. \frac{dE}{dx} \right|_i, \quad (1.24)$$

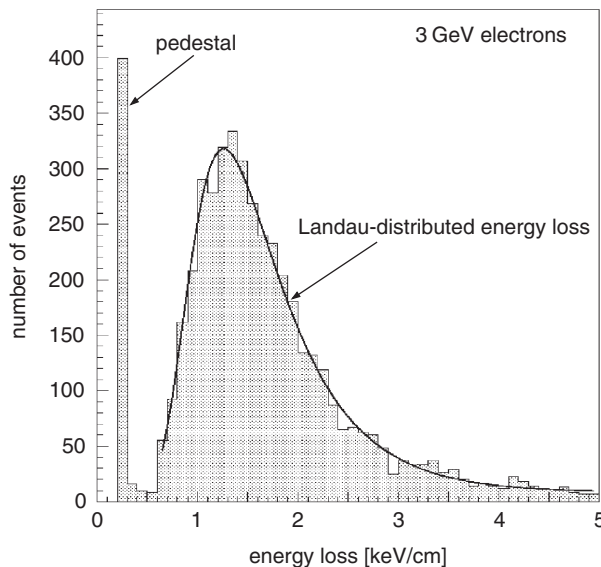


Fig. 1.3. Energy-loss distribution of 3 GeV electrons in a thin-gap drift chamber filled with Ar/CH₄ (80:20) [23].

where f_i is the mass fraction of the i th element and $\left. \frac{dE}{dx} \right|_i$, the average energy loss in this element. Corrections to this relation because of the dependence of the ionisation constant on the molecular structure can be safely neglected.

The energy transfers to ionisation electrons can be so large that these electrons can cause further ionisation. These electrons are called δ rays or knock-on electrons. The energy spectrum of knock-on electrons is given by [1, 10–12, 25]

$$\frac{dN}{dE_{\text{kin}}} = \xi \cdot \frac{F}{E_{\text{kin}}^2} \quad (1.25)$$

for $I \ll E_{\text{kin}} \leq E_{\text{kin}}^{\text{max}}$.

F is a spin-dependent factor of order unity, if $E_{\text{kin}} \ll E_{\text{kin}}^{\text{max}}$ [12]. Of course, the energy spectrum of knock-on electrons falls to zero if the maximum transferable energy is reached. This kinematic limit also constrains the factor F [1, 25]. The spin dependence of the spectrum of the knock-on electrons only manifests itself close to the maximum transferable energy [1, 25].

The strong fluctuations of the energy loss in thin absorber layers are quite frequently not observed by a detector. Detectors only measure the energy which is actually deposited in their sensitive volume, and this energy may not be the same as the energy lost by the particle. For example, the energy which is transferred to knock-on electrons may only be partially deposited in the detector because the knock-on electrons can leave the sensitive volume of the detector.

Therefore, quite frequently it is of practical interest to consider only that part of the energy loss with energy transfers E smaller than a given cut value E_{cut} . This *truncated energy loss* is given by [10–12, 26]

$$-\left. \frac{dE}{dx} \right|_{\leq E_{\text{cut}}} = \kappa \left(\ln \frac{2m_e c^2 \beta^2 \gamma^2 E_{\text{cut}}}{I^2} - \beta^2 - \delta \right), \quad (1.26)$$

where κ is defined by Eq. (1.13). Equation (1.26) is similar, but not identical, to Eq. (1.11). Distributions of the truncated energy loss do not show a pronounced Landau tail as the distributions (1.19) for the mean value (1.11). Because of the density effect – expressed by δ in Eqs. (1.11) or (1.26), respectively – the truncated energy loss approaches a constant at high energies, which is given by the Fermi plateau.

So far, the energy loss by ionisation and excitation has been described for heavy particles. Electrons as incident particles, however, play a special rôle in the treatment of the energy loss. On the one hand, the total energy loss of electrons even at low energies (MeV range) is influenced by bremsstrahlung processes. On the other hand, the ionisation loss requires

special treatment because the mass of the incident particle and the target electron is the same.

In this case, one can no longer distinguish between the primary and secondary electron after the collision. Therefore, the energy-transfer probability must be interpreted in a different manner. One electron after the collision receives the energy E_{kin} and the other electron the energy $E - m_e c^2 - E_{\text{kin}}$ (E is the total energy of the incident particle). All possible cases are considered if one allows the energy transfer to vary between 0 and $\frac{1}{2}(E - m_e c^2)$ and not up to $E - m_e c^2$.

This effect can be most clearly seen if in Eq. (1.11) the maximum energy transfer $E_{\text{kin}}^{\text{max}}$ of Eq. (1.6) is replaced by the corresponding expression for electrons. For relativistic particles, the term $\frac{1}{2}(E - m_e c^2)$ can be approximated by $E/2 = \frac{1}{2}\gamma m_e c^2$. Using $z = 1$, the ionisation loss of electrons then can be approximated by

$$-\frac{dE}{dx} = 4\pi N_A r_e^2 m_e c^2 \frac{Z}{A} \cdot \frac{1}{\beta^2} \left(\ln \frac{\gamma m_e c^2}{2I} - \beta^2 - \frac{\delta^*}{2} \right), \quad (1.27)$$

where δ^* takes a somewhat different value for electrons compared to the parameter δ appearing in Eq. (1.11). A more precise calculation considering the specific differences between incident heavy particles and electrons yields a more exact formula for the energy loss of electrons due to ionisation and excitation [27],

$$-\frac{dE}{dx} = 4\pi N_A r_e^2 m_e c^2 \frac{Z}{A} \cdot \frac{1}{\beta^2} \left[\ln \frac{\gamma m_e c^2 \beta \sqrt{\gamma - 1}}{\sqrt{2}I} + \frac{1}{2}(1 - \beta^2) - \frac{2\gamma - 1}{2\gamma^2} \ln 2 + \frac{1}{16} \left(\frac{\gamma - 1}{\gamma} \right)^2 \right]. \quad (1.28)$$

This equation agrees with the general Bethe–Bloch relation (1.11) within 10%–20%. It takes into account the kinematics of electron–electron collisions and also screening effects.

The treatment of the ionisation loss of positrons is similar to that of electrons if one considers that these particles are of equal mass, but not identical charge.

For completeness, we also give the ionisation loss of positrons [28]:

$$-\frac{dE}{dx} = 4\pi N_A r_e^2 m_e c^2 \frac{Z}{A} \frac{1}{\beta^2} \left\{ \ln \frac{\gamma m_e c^2 \beta \sqrt{\gamma - 1}}{\sqrt{2}I} - \frac{\beta^2}{24} \left[23 + \frac{14}{\gamma + 1} + \frac{10}{(\gamma + 1)^2} + \frac{4}{(\gamma + 1)^3} \right] \right\}. \quad (1.29)$$

Since positrons are antiparticles of electrons, there is, however, an additional consideration: if positrons come to rest, they will annihilate with

an electron normally into two photons which are emitted anticollinearly. Both photons have energies of 511 keV in the centre-of-mass system, corresponding to the rest mass of the electrons. The *cross section for annihilation* in flight is given by [28]

$$\sigma(Z, E) = \frac{Z\pi r_e^2}{\gamma + 1} \left[\frac{\gamma^2 + 4\gamma + 1}{\gamma^2 - 1} \ln(\gamma + \sqrt{\gamma^2 - 1}) - \frac{\gamma + 3}{\sqrt{\gamma^2 - 1}} \right]. \quad (1.30)$$

More details about the ionisation process of elementary particles, in particular, its spin dependence, can be taken from the books of Rossi and Sitar *et al.* [1–3].

1.1.2 Channelling

The energy loss of charged particles as described by the Bethe–Bloch formula needs to be modified for crystals where the collision partners are arranged on a regular lattice. By looking into a crystal it becomes immediately clear that the energy loss along certain crystal directions will be quite different from that along a non-aligned direction or in an amorphous substance. The motion along such channelling directions is governed mainly by coherent scattering on strings and planes of atoms rather than by the individual scattering off single atoms. This leads to anomalous energy losses of charged particles in crystalline materials [29].

It is obvious from the crystal structure that charged particles can only be channelled along a crystal direction if they are moving more or less parallel to crystal axes. The critical angle necessary for *channelling* is small (approx. 0.3° for $\beta \approx 0.1$) and decreases with energy. For the axial direction ($\langle 111 \rangle$, body diagonal) it can be estimated by

$$\psi [\text{degrees}] = 0.307 \cdot [z \cdot Z / (E \cdot d)]^{0.5}, \quad (1.31)$$

where z and Z are the charges of the incident particle and the crystal atom, E is the particle's energy in MeV, and d is the interatomic spacing in Å. ψ is measured in degrees [30].

For protons ($z = 1$) passing through a silicon crystal ($Z = 14$; $d = 2.35$ Å), the critical angle for channelling along the direction-of-body diagonals becomes

$$\psi = 13 \mu\text{rad} / \sqrt{E [\text{TeV}]} . \quad (1.32)$$

For planar channelling along the face diagonals ($\langle 110 \rangle$ axis) in silicon one gets [29]

$$\psi = 5 \mu\text{rad} / \sqrt{E [\text{TeV}]} . \quad (1.33)$$

Of course, the channelling process also depends on the charge of the incident particle.

For a field inside a crystal of silicon atoms along the $\langle 110 \rangle$ crystal direction, one obtains a value of $1.3 \cdot 10^{10}$ V/cm. This field extends over macroscopic distances and can be used for the deflection of high-energy charged particles using bent crystals [30].

Channelled positive particles are kept away from a string of atoms and consequently suffer a relatively small energy loss. Figure 1.4 shows the energy-loss spectra for 15 GeV/c protons passing through a 740 μm thick germanium crystal [30]. The energy loss of channelled protons is lower by about a factor of 2 compared to random directions through the crystal.

1.1.3 Ionisation yield

The average energy loss by ionisation and excitation can be transformed into a number of electron–ion pairs produced along the track of a charged particle. One must distinguish between *primary ionisation*, that is the number of primarily produced electron–ion pairs, and the *total ionisation*. A sufficiently large amount of energy can be transferred to some primarily produced electrons so that they also can ionise (knock-on electrons). This secondary ionisation together with the primary ionisation forms the total ionisation.

The average energy required to form an electron–ion pair (W value) exceeds the ionisation potential of the gas because, among others, inner shells of the gas atoms can also be involved in the ionisation process,

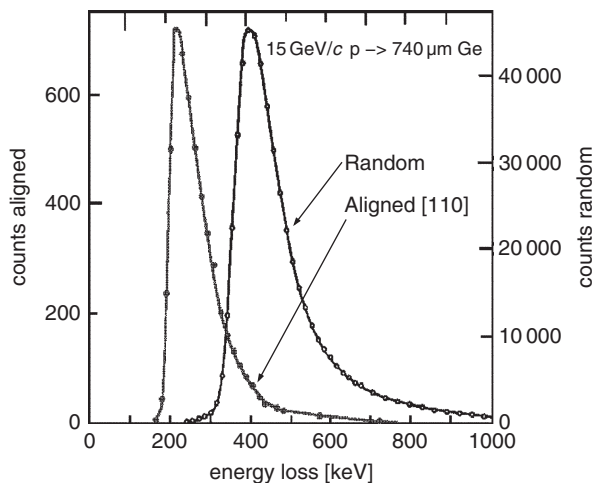


Fig. 1.4. The energy-loss spectra for 15 GeV/c protons passing through a 740 μm thick germanium crystal [30].

Table 1.2. *Compilation of some properties of gases. Given is the average effective ionisation potential per electron I_0 , the average energy loss W per produced ion pair, the number of primary (n_p), and total (n_T) produced electron–ion pairs per cm at standard pressure and temperature for minimum-ionising particles [10, 11, 31–33]*

Gas	Density ρ [g/cm ³]	I_0 [eV]	W [eV]	n_p [cm ⁻¹]	n_T [cm ⁻¹]
H ₂	$8.99 \cdot 10^{-5}$	15.4	37	5.2	9.2
He	$1.78 \cdot 10^{-4}$	24.6	41	5.9	7.8
N ₂	$1.25 \cdot 10^{-3}$	15.5	35	10	56
O ₂	$1.43 \cdot 10^{-3}$	12.2	31	22	73
Ne	$9.00 \cdot 10^{-4}$	21.6	36	12	39
Ar	$1.78 \cdot 10^{-3}$	15.8	26	29	94
Kr	$3.74 \cdot 10^{-3}$	14.0	24	22	192
Xe	$5.89 \cdot 10^{-3}$	12.1	22	44	307
CO ₂	$1.98 \cdot 10^{-3}$	13.7	33	34	91
CH ₄	$7.17 \cdot 10^{-4}$	13.1	28	16	53
C ₄ H ₁₀	$2.67 \cdot 10^{-3}$	10.8	23	46	195

and a fraction of the energy of the incident particle can be dissipated by excitation processes which do not lead to free electrons. The W value of a material is constant for relativistic particles and increases only slightly for low velocities of incident particles.

For gases, the W values are around 30 eV. They can, however, strongly depend on impurities in the gas. Table 1.2 shows the W values for some gases together with the number of primary (n_p) and total (n_T) electron–ion pairs produced by minimum-ionising particles (see Table 1.1) [10, 11, 31–33].

The numerical values for n_p are somewhat uncertain because experimentally it is very difficult to distinguish between primary and secondary ionisation. The total ionisation (n_T) can be computed from the total energy loss ΔE in the detector according to

$$n_T = \frac{\Delta E}{W} . \quad (1.34)$$

This is only true if the transferred energy is completely deposited in the sensitive volume of the detector.

In solid-state detectors, charged particles produce *electron–hole pairs*. For the production of an electron–hole pair on the average 3.6 eV in silicon and 2.85 eV in germanium are required. This means that the number

of charge carriers produced in solid-state detectors is much larger compared to the production rate of electron–ion pairs in gases. Therefore, the statistical fluctuations in the number of produced charge carriers for a given energy loss is much smaller in solid-state detectors than in gaseous detectors.

The production of pairs of charge carriers for a given energy loss is a statistical process. If, on average, N charge-carrier pairs are produced one would naïvely expect this number to fluctuate according to Poisson statistics with an error of \sqrt{N} . Actually, the fluctuation around the average value is smaller by a factor \sqrt{F} depending on the material; this was demonstrated for the first time by Fano [34]. If one considers the situation in detail, the origin of the *Fano factor* is clear. For a given energy deposit, the number of produced charge carriers is limited by energy conservation.

In the following, a formal justification for the Fano factor will be given [34, 35]. Let $E = E_{\text{total}}$ be the fixed energy deposited in a detector, e.g. by an X-ray photon or a stopping α particle. This energy is transferred in p steps to the detector medium, in general, in unequal portions E_p in each individual ionisation process. For each interaction step, m_p electron–ion pairs are produced. After N steps, the total energy is completely absorbed (Fig. 1.5).

Let

$m_p^{(e)} = \frac{E_p}{W}$ be the expected number of ionisations in the step p , and

$\bar{n}^{(e)} = \frac{E}{W}$ be the average expected number of the totally produced electron–ion pairs.

The quantity, which will finally describe the energy resolution, is

$$\sigma^2 = \langle (n - \bar{n})^2 \rangle , \quad (1.35)$$

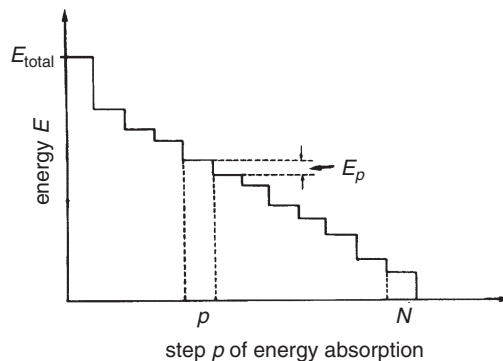


Fig. 1.5. Energy loss in N discrete steps with energy transfer E_p in the p th step [35].

where \bar{n} is the average value over many experiments for fixed energy absorption:

$$\sigma^2 = \frac{1}{L} \sum_{k=1}^L (n_k - \bar{n})^2 . \quad (1.36)$$

That is, we perform L gedanken experiments, where in experiment k a total number n_k electron-ion pairs is produced. In experiment k the energy is transferred to the detector medium in N_k steps, where in the p th interval the number of produced electron-ion pairs is m_{pk} ;

$$n_k - \bar{n} = \sum_{p=1}^{N_k} m_{pk} - \frac{E}{W} = \sum_{p=1}^{N_k} m_{pk} - \frac{1}{W} \sum_{p=1}^{N_k} E_{pk} . \quad (1.37)$$

The second term in the sum constrains the statistical character of the charge-carrier production rate through energy conservation. Therefore, one would expect that the fluctuations are smaller compared to an unconstrained accidental energy-loss process.

The energy E is subdivided consequently into N_k discrete steps each with energy portion E_{pk} . If we introduce

$$\nu_{pk} = m_{pk} - \frac{E_{pk}}{W} , \quad (1.38)$$

it follows that

$$n_k - \bar{n} = \sum_{p=1}^{N_k} \nu_{pk} . \quad (1.39)$$

The variance for L experiments is given by

$$\sigma^2(n) = \frac{1}{L} \cdot \underbrace{\sum_{k=1}^L}_{L \text{ experiments}} \underbrace{\left(\sum_{p=1}^{N_k} \nu_{pk} \right)^2}_{\text{per experiment}} , \quad (1.40)$$

$$\sigma^2(n) = \frac{1}{L} \left(\sum_{k=1}^L \sum_{p=1}^{N_k} \nu_{pk}^2 + \sum_{k=1}^L \sum_{i \neq j}^{N_k} \nu_{ik} \nu_{jk} \right) . \quad (1.41)$$

Let us consider the mixed term at first:

$$\frac{1}{L} \sum_{k=1}^L \sum_{i \neq j}^{N_k} \nu_{ik} \nu_{jk} = \frac{1}{L} \sum_{k=1}^L \sum_{i=1}^{N_k} \nu_{ik} \left(\sum_{j=1}^{N_k} \nu_{jk} - \nu_{ik} \right) . \quad (1.42)$$

The last term in the bracket of Eq. (1.42) originates from the suppression of the product $\nu_{ik}\nu_{jk}$ for $i = j$, which is already contained in the quadratic terms.

For a given event k the average value

$$\bar{\nu}_k = \frac{1}{N_k} \sum_{j=1}^{N_k} \nu_{jk} \tag{1.43}$$

can be introduced. Using this quantity, one gets

$$\frac{1}{L} \sum_{k=1}^L \sum_{i \neq j}^{N_k} \nu_{ik}\nu_{jk} = \frac{1}{L} \sum_{k=1}^L N_k \bar{\nu}_k (N_k \bar{\nu}_k - \bar{\nu}_k) . \tag{1.44}$$

In this equation the last term ν_{ik} has been approximated by the average value $\bar{\nu}_k$. Under these conditions one obtains

$$\frac{1}{L} \sum_{k=1}^L \sum_{i \neq j}^{N_k} \nu_{ik}\nu_{jk} = \frac{1}{L} \sum_{k=1}^L N_k (N_k - 1) \bar{\nu}_k^2 = (\overline{N^2} - \bar{N}) \bar{\nu}^2 , \tag{1.45}$$

if one assumes that N_k and $\bar{\nu}_k$ are uncorrelated, and $\bar{\nu}_k = \bar{\nu}$, if N_k is sufficiently large.

The average value of ν , however, vanishes according to Eq. (1.38), consequently the second term in Eq. (1.41) does not contribute. The remaining first term gives

$$\sigma^2(n) = \frac{1}{L} \sum_{k=1}^L \sum_{p=1}^{N_k} \nu_{pk}^2 = \frac{1}{L} \sum_{k=1}^L N_k \overline{\nu_k^2} = \overline{N \nu^2} = \bar{N} \cdot \overline{(m_p - E_p/W)^2} . \tag{1.46}$$

In this case m_p is the actually measured number of electron-ion pairs in the energy-absorption step p with energy deposit E_p .

Remembering that $\bar{N} = \frac{\bar{n}}{\bar{m}_p}$, leads to

$$\sigma^2(n) = \frac{\overline{(m_p - E_p/W)^2}}{\bar{m}_p} \bar{n} . \tag{1.47}$$

The variance of n consequently is

$$\sigma^2(n) = F \cdot \bar{n} \tag{1.48}$$

with the Fano factor

$$F = \frac{\overline{(m_p - E_p/W)^2}}{\bar{m}_p} . \tag{1.49}$$

Table 1.3. *Fano factors for typical detector materials at 300 K [35, 36]*

Absorber	F
Ar + 10% CH ₄	≈ 0.2
Si	0.12
Ge	0.13
GaAs	0.10
Diamond	0.08

As a consequence, the energy resolution is improved by the factor \sqrt{F} compared to Poisson fluctuations. However, it must be remembered that one has to distinguish between the occasional very large fluctuations of the energy loss (Landau fluctuations) in thin absorber layers and the fluctuation of the number of produced electron–ion pairs for a given fixed well-defined energy loss. This last case is true for all particles which deposit their total energy in the sensitive volume of the detector.

Table 1.3 lists some Fano factors for various substances at 300 K [35, 36]. The improvement on the energy resolution can be quite substantial.

1.1.4 Multiple scattering

A charged particle traversing matter will be scattered by the Coulomb potentials of nuclei and electrons. In contrast to the ionisation energy loss which is caused by collisions with atomic electrons, multiple-scattering processes are dominated by deflections in the Coulomb field of nuclei. This leads to a large number of scattering processes with very low deviations from the original path. The distribution of scattering angles due to multiple *Coulomb scattering* is described by *Molière's theory* [10–12, 37]. For small scattering angles it is normally distributed around the average scattering angle $\Theta = 0$. Larger scattering angles caused by collisions of charged particles with nuclei are, however, more frequent than expected from a Gaussian distribution [38].

The root mean square of the projected *scattering-angle distribution* is given by [10–12]

$$\Theta_{\text{rms}}^{\text{proj.}} = \sqrt{\langle \Theta^2 \rangle} = \frac{13.6 \text{ MeV}}{\beta c p} z \sqrt{\frac{x}{X_0}} [1 + 0.038 \ln(x/X_0)] , \quad (1.50)$$

where p (in MeV/ c) is the momentum, βc the velocity, and z the charge of the scattered particle. x/X_0 is the thickness of the scattering

medium, measured in units of the radiation length (see Sect. 1.1.5) [1, 39, 40]

$$X_0 = \frac{A}{4\alpha N_A Z^2 r_e^2 \ln(183 Z^{-1/3})} , \quad (1.51)$$

where Z and A are the atomic number and the atomic weight of the absorber, respectively.

Equation (1.50) is already an approximation. For most practical applications Eq. (1.50) can be further approximated for particles with $z = 1$ by

$$\Theta_{\text{rms}}^{\text{proj.}} = \sqrt{\langle \Theta^2 \rangle} \approx \frac{13.6 \text{ MeV}}{\beta c p} \sqrt{\frac{x}{X_0}} . \quad (1.52)$$

Equation (1.50) or (1.52) gives the root mean square of the projected distribution of the scattering angles. Such a projected distribution is, for example, of interest for detectors, which provide only a two-dimensional view of an event. The corresponding root mean square deviation for non-projected scattering angles is increased by factor $\sqrt{2}$ so that we have

$$\Theta_{\text{rms}}^{\text{space}} \approx \frac{19.2 \text{ MeV}}{\beta c p} \sqrt{\frac{x}{X_0}} . \quad (1.53)$$

1.1.5 Bremsstrahlung

Fast charged particles lose, in addition to their ionisation loss, energy by interactions with the Coulomb field of the nuclei of the traversed medium. If the charged particles are decelerated in the Coulomb field of the nucleus, a fraction of their kinetic energy will be emitted in form of photons (*bremsstrahlung*).

The energy loss by bremsstrahlung for high energies can be described by [1]

$$-\frac{dE}{dx} \approx 4\alpha \cdot N_A \cdot \frac{Z^2}{A} \cdot z^2 \left(\frac{1}{4\pi\epsilon_0} \cdot \frac{e^2}{mc^2} \right)^2 \cdot E \ln \frac{183}{Z^{1/3}} . \quad (1.54)$$

In this equation

Z, A – are the atomic number and atomic weight of the medium,
 z, m, E – are the charge number, mass and energy of the incident particle.

The bremsstrahlung energy loss of electrons is given correspondingly by

$$-\frac{dE}{dx} \approx 4\alpha N_A \cdot \frac{Z^2}{A} r_e^2 \cdot E \ln \frac{183}{Z^{1/3}} \quad (1.55)$$

if $E \gg m_e c^2 / \alpha Z^{1/3}$.

It should be pointed out that, in contrast to the ionisation energy loss, Eq. (1.11), the energy loss by bremsstrahlung is proportional to the energy of the particle and inversely proportional to the mass squared of the incident particles.

Because of the smallness of the electron mass, bremsstrahlung energy losses play an especially important rôle for electrons. For electrons ($z = 1$, $m = m_e$) Eq. (1.54) or Eq. (1.55), respectively, can be written in the following fashion:

$$-\frac{dE}{dx} = \frac{E}{X_0} . \quad (1.56)$$

This equation defines the *radiation length* X_0 . An approximation for X_0 has already been given by Eq. (1.51).

The proportionality

$$X_0^{-1} \propto Z^2 \quad (1.57)$$

in Eq. (1.51) originates from the interaction of the incident particle with the Coulomb field of the target nucleus.

Bremsstrahlung, however, is also emitted in interactions of incident particles with the electrons of the target material. The cross section for this process follows closely the calculation of the bremsstrahlung energy loss on the target nucleus, the only difference being that for atomic target electrons the charge is always equal to unity, and therefore one obtains an additional contribution to the cross section, which is proportional to the number of target electrons, that is $\propto Z$. The cross section for bremsstrahlung must be extended by this term [9]. Therefore, the factor Z^2 in Eq. (1.51) must be replaced by $Z^2 + Z = Z(Z+1)$, which leads to a better description of the radiation length, accordingly,[†]

$$X_0 = \frac{A}{4\alpha N_A Z(Z+1)r_e^2 \ln(183 Z^{-1/3})} \{g/cm^2\} . \quad (1.58)$$

In addition, one has to consider that the atomic electrons will screen the Coulomb field of the nucleus to a certain extent. If *screening effects*

[†] Units presented in curly brackets just indicate that the numerical result of the formula is given in the units shown in the brackets, i.e., in this case the radiation length comes out in g/cm².

are taken into account, the radiation length can be approximated by [10–12]

$$X_0 = \frac{716.4 \cdot A[\text{g/mol}]}{Z(Z+1) \ln(287/\sqrt{Z})} \text{ g/cm}^2 . \quad (1.59)$$

The numerical results for the radiation length based on Eq. (1.59) deviate from those of Eq. (1.51) by a few per cent.

The radiation length X_0 is a property of the material. However, one can also define a radiation length for incident particles other than electrons. Because of the proportionality

$$X_0 \propto r_e^{-2} \quad (1.60)$$

and the relation

$$r_e = \frac{1}{4\pi\epsilon_0} \cdot \frac{e^2}{m_e c^2} , \quad (1.61)$$

the ‘radiation length’, however, also has a dependence on the mass of the incident particle,

$$\tilde{X}_0 \propto m^2 . \quad (1.62)$$

The radiation lengths given in the literature, however, are always meant for electrons.

Integrating Eq. (1.54) or (1.56), respectively, leads to

$$E = E_0 e^{-x/X_0} . \quad (1.63)$$

This function describes the exponential attenuation of the *energy* of charged particles by radiation losses. Note the distinction from the exponential attenuation of the *intensity* of a photon beam passing through matter (see Sect. 1.2, Eq. (1.92)).

The radiation length of a mixture of elements or a compound can be approximated by

$$X_0 = \frac{1}{\sum_{i=1}^N f_i / X_0^i} , \quad (1.64)$$

where f_i are the mass fractions of the components with the radiation length X_0^i .

Energy losses due to bremsstrahlung are proportional to the energy while ionisation energy losses beyond the minimum of ionisation are proportional to the logarithm of the energy. The energy, where these two interaction processes for electrons lead to equal energy losses, is called the *critical energy* E_c ,

$$-\frac{dE}{dx}(E_c) \Big|_{\text{ionisation}} = -\frac{dE}{dx}(E_c) \Big|_{\text{bremsstrahlung}} . \quad (1.65)$$

The energy distribution of bremsstrahlung photons follows a $1/E_\gamma$ law (E_γ – energy of the emitted photon). The photons are emitted preferentially in the forward direction ($\Theta_\gamma \approx m_e c^2/E$). In principle, the critical energy can be calculated from the Eqs. (1.11) and (1.54) using Eq. (1.65). Numerical values for the critical energy of electrons are given in the literature [9–11]. For solids the equation

$$E_c = \frac{610 \text{ MeV}}{Z + 1.24} \quad (1.66)$$

describes the critical energies quite satisfactorily [41]. Similar parametrisations for gases, liquids and solids are given in [12]. The critical energy is related to the radiation length by

$$\left(\frac{dE}{dx}\right) \cdot X_0 \approx E_c . \quad (1.67)$$

Table 1.4 lists the radiation lengths and critical energies for some materials [9–12]. The critical energy – as well as the radiation length – scales as the square of the mass of the incident particles. For muons ($m_\mu = 106 \text{ MeV}/c^2$) in iron one obtains:

$$E_c^\mu \approx E_c^e \cdot \left(\frac{m_\mu}{m_e}\right)^2 = 890 \text{ GeV} . \quad (1.68)$$

1.1.6 Direct electron-pair production

Apart from bremsstrahlung losses, additional energy-loss mechanisms come into play, particularly at high energies. Electron–positron pairs can be produced by virtual photons in the Coulomb field of the nuclei. For high-energy muons this energy-loss mechanism is even more important than bremsstrahlung losses. The energy loss by *trident production* (e.g. like $\mu + \text{nucleus} \rightarrow \mu + e^+ + e^- + \text{nucleus}$) is also proportional to the energy and can be parametrised by

$$-\frac{dE}{dx} \Big|_{\text{pair pr.}} = b_{\text{pair}}(Z, A, E) \cdot E ; \quad (1.69)$$

Table 1.4. Radiation lengths and critical energies for some absorber materials [9–12]. The values for the radiation lengths agree with Eq. (1.59) within a few per cent. Only the experimental value for helium shows a somewhat larger deviation. The numerical results for the critical energies of electrons scatter quite significantly in the literature. The effective values for Z and A of mixtures and compounds can be calculated for A by $A_{\text{eff}} = \sum_{i=1}^N f_i A_i$, where f_i are the mass fractions of the components with atomic weight A_i . Correspondingly, one obtains the effective atomic numbers using Eqs. (1.59) and (1.64). Neglecting the logarithmic Z dependence in Eq. (1.59), Z_{eff} can be calculated from $Z_{\text{eff}} \cdot (Z_{\text{eff}} + 1) = \sum_{i=1}^N f_i Z_i (Z_i + 1)$, where f_i are the mass fractions of the components with charge numbers Z_i . For the practical calculation of an effective radiation length of a compound one determines first the radiation length of the contributing components and then determines the effective radiation length according to Eq. (1.64)

Material	Z	A	X_0 [g/cm ²]	X_0 [cm]	E_c [MeV]
Hydrogen	1	1.01	61.3	731 000	350
Helium	2	4.00	94	530 000	250
Lithium	3	6.94	83	156	180
Carbon	6	12.01	43	18.8	90
Nitrogen	7	14.01	38	30 500	85
Oxygen	8	16.00	34	24 000	75
Aluminium	13	26.98	24	8.9	40
Silicon	14	28.09	22	9.4	39
Iron	26	55.85	13.9	1.76	20.7
Copper	29	63.55	12.9	1.43	18.8
Silver	47	109.9	9.3	0.89	11.9
Tungsten	74	183.9	6.8	0.35	8.0
Lead	82	207.2	6.4	0.56	7.40
Air	7.3	14.4	37	30 000	84
SiO ₂	11.2	21.7	27	12	57
Water	7.5	14.2	36	36	83

the $b(Z, A, E)$ parameter varies only slowly with energy for high energies. For 100 GeV muons in iron the energy loss due to *direct electron-pair production* can be described by [25, 42, 43]

$$-\left. \frac{dE}{dx} \right|_{\text{pair pr.}} = 3 \cdot 10^{-6} \cdot \frac{E}{\text{MeV}} \frac{\text{MeV}}{\text{g/cm}^2}, \quad (1.70)$$

$$\text{i.e. } -\left. \frac{dE}{dx} \right|_{\text{pair pr.}} = 0.3 \frac{\text{MeV}}{\text{g/cm}^2}. \quad (1.71)$$

The spectrum of total energy of directly produced electron–positron pairs at high energy transfers is steeper than the spectrum of bremsstrahlung photons. High fractional energy transfers are therefore dominated by bremsstrahlung processes [25].

1.1.7 Energy loss by photonuclear interactions

Charged particles can interact inelastically via virtual gauge particles (in this case, photons) with nuclei of the absorber material, thereby losing energy (nuclear interactions).

In the same way as for energy losses through bremsstrahlung or direct electron-pair production, the energy loss by *photonuclear interactions* is proportional to the particle's energy,

$$-\left. \frac{dE}{dx} \right|_{\text{photonucl.}} = b_{\text{nucl.}}(Z, A, E) \cdot E . \quad (1.72)$$

For 100 GeV muons in iron the energy-loss parameter b is given by $b_{\text{nucl.}} = 0.4 \cdot 10^{-6} \text{ g}^{-1} \text{ cm}^2$ [25], i.e.,

$$-\left. \frac{dE}{dx} \right|_{\text{photonucl.}} = 0.04 \frac{\text{MeV}}{\text{g/cm}^2} . \quad (1.73)$$

This energy loss is important for leptons and negligible for hadrons in comparison to direct nuclear interactions.

1.1.8 Total energy loss

In contrast to energy losses due to ionisation those by bremsstrahlung, direct electron-pair production and photonuclear interactions are characterised by large energy transfers with correspondingly large fluctuations. Therefore, it is somewhat problematic to speak of an average energy loss for these processes because extremely large fluctuations around this average value can occur [44, 45].

Nevertheless, the total energy loss of charged particles by the above mentioned processes can be parametrised by

$$\begin{aligned} -\left. \frac{dE}{dx} \right|_{\text{total}} &= -\left. \frac{dE}{dx} \right|_{\text{ionisation}} - \left. \frac{dE}{dx} \right|_{\text{brems.}} - \left. \frac{dE}{dx} \right|_{\text{pair pr.}} - \left. \frac{dE}{dx} \right|_{\text{photonucl.}} \\ &= a(Z, A, E) + b(Z, A, E) \cdot E , \end{aligned} \quad (1.74)$$

where $a(Z, A, E)$ describes the energy loss according to Eq. (1.11) and $b(Z, A, E)$ is the sum over the energy losses due to bremsstrahlung, direct electron-pair production and photonuclear interactions. The parameters

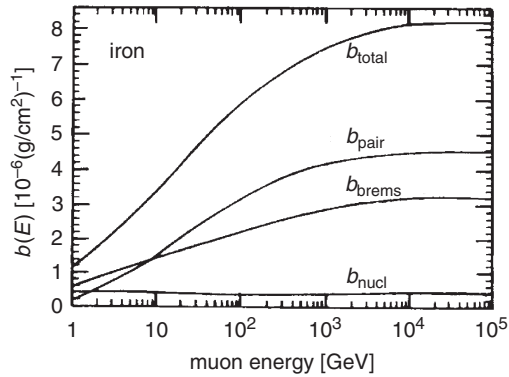


Fig. 1.6. Variation of the b parameters with energy for muons in iron. Plotted are the fractional energy losses by direct electron-pair production (b_{pair}), bremsstrahlung (b_{brems}), and photonuclear interactions (b_{nucl}), as well as their sum (b_{total}) [42].

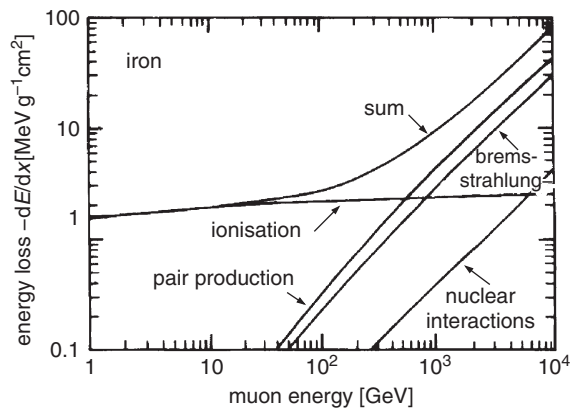


Fig. 1.7. Contributions to the energy loss of muons in iron [42].

a and b and their energy dependence for various particles and materials are given in the literature [46].

Figure 1.6 shows the b parameters and in Fig. 1.7 the various energy-loss mechanisms for muons in iron in their dependence on the muon energy are presented [42].

Up to energies of several hundred GeV the energy loss in iron due to ionisation and excitation is dominant. For energies in excess of several TeV direct electron-pair production and bremsstrahlung represent the main energy-loss processes. Photonuclear interactions contribute only at the 10% level. Since the energy loss due to these processes is proportional

to the muon's energy, this opens up the possibility of muon calorimetry by means of energy-loss sampling [47].

The dominance of the energy-proportional interaction processes over ionisation and excitation depends, of course, on the target material. For uranium this transition starts around several 100 GeV, while in hydrogen bremsstrahlung and direct electron-pair production prevail only at energies in excess of 10 TeV.

1.1.9 Energy-range relations for charged particles

Because of the different energy-loss mechanisms, it is nearly impossible to give a simple representation of the range of charged particles in matter. The definition of a range is in any case complicated because of the fluctuations of the energy loss by catastrophic energy-loss processes, i.e. by interactions with high energy transfers, and because of the multiple Coulomb scattering in the material, all of which lead to substantial range straggling. In the following, therefore, some empirical formulae are given, which are valid for certain particle species in fixed energy ranges.

Generally speaking, the range can be calculated from:

$$R = \int_E^{m_0c^2} \frac{dE}{dE/dx} . \quad (1.75)$$

However, since the energy loss is a complicated function of the energy, in most cases approximations of this integral are used. For the determination of the range of low-energy particles, in particular, the difference between the total energy E and the kinetic energy E_{kin} must be taken into account, because only the kinetic energy can be transferred to the material.

For α particles with kinetic energies between $2.5 \text{ MeV} \leq E_{\text{kin}} \leq 20 \text{ MeV}$ the range in air (15°C , 760 Torr) can be described by [48]

$$R_\alpha = 0.31(E_{\text{kin}}/\text{MeV})^{3/2} \text{ cm} . \quad (1.76)$$

For rough estimates of the range of α particles in other materials one can use

$$R_\alpha = 3.2 \cdot 10^{-4} \frac{\sqrt{A/(\text{g/mol})}}{\rho/(\text{g cm}^{-3})} \cdot R_{\text{air}} \{\text{cm}\} \quad (1.77)$$

(A atomic weight) [48]. The range of α particles in air is shown in Fig. 1.8.

For protons with kinetic energies between $0.6 \text{ MeV} \leq E_{\text{kin}} \leq 20 \text{ MeV}$ the range in air [48] can be approximated by

$$R_p = 100 \cdot \left(\frac{E_{\text{kin}}}{9.3 \text{ MeV}} \right)^{1.8} \text{ cm} . \quad (1.78)$$

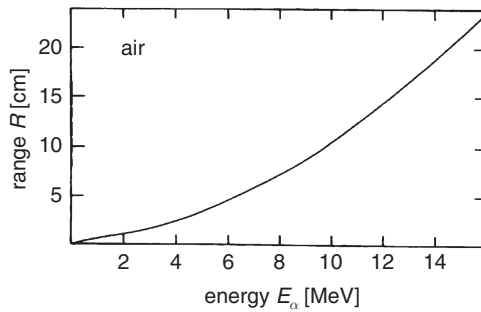
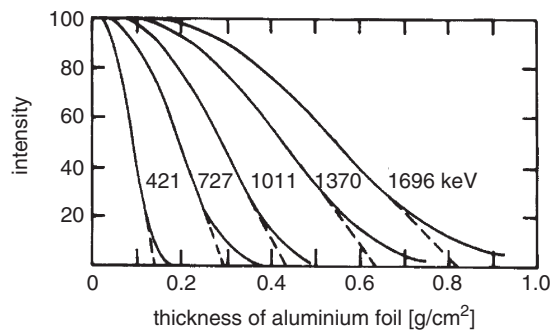
Fig. 1.8. Range of α particles in air [48].

Fig. 1.9. Absorption of electrons in aluminium [49, 50].

The range of low-energy electrons ($0.5 \text{ MeV} \leq E_{\text{kin}} \leq 5 \text{ MeV}$) in aluminium is described [48] by

$$R_e = 0.526 (E_{\text{kin}}/\text{MeV} - 0.094) \text{ g/cm}^2 . \quad (1.79)$$

Figure 1.9 shows the absorption of electrons in aluminium [49, 50]. Plotted is the fraction of electrons (with the energy E_{kin}), which penetrate through a certain absorber thickness.

This figure shows the difficulty in the definition of a range of a particle due to the pronounced range straggling, in this case mainly due to the fact that electrons will experience multiple scattering and will bremsstrahl in the absorber. For particles heavier than the electron the range is much better defined due to the reduced effect of multiple scattering ($\langle \Theta^2 \rangle \propto 1/p$). The extrapolation of the linear part of the curves shown in Fig. 1.9 to the intersection with the abscissa defines the *practical range* [50]. The range of electrons defined in this way is shown in Fig. 1.10 for various absorbers [50].

For higher energies the range of muons, pions and protons can be taken from Fig. 1.11 [12].

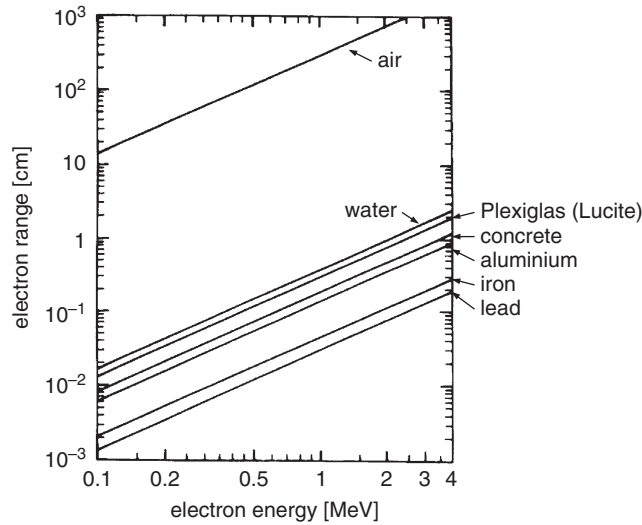


Fig. 1.10. Practical range of electrons in various materials [50].

The range of high-energy muons can be obtained by integrating Eq. (1.75), using Eqs. (1.74) and (1.11), and neglecting the logarithmic term in Eq. (1.11). This leads to

$$R_\mu(E_\mu) = \frac{1}{b} \ln \left(1 + \frac{b}{a} E_\mu \right) . \tag{1.80}$$

For 1 TeV muons in iron Eq. (1.80) yields

$$R_\mu(1 \text{ TeV}) = 265 \text{ m} . \tag{1.81}$$

A numerical integration for the range of muons in rock (standard rock with $Z = 11$, $A = 22$) yields for $E_\mu > 10 \text{ GeV}$ [51]

$$R_\mu(E_\mu) = \left[\frac{1}{b} \ln \left(1 + \frac{b}{a} E_\mu \right) \right] \left(0.96 \frac{\ln E_{\mu,n} - 7.894}{\ln E_{\mu,n} - 8.074} \right) \tag{1.82}$$

with $a = 2.2 \frac{\text{MeV}}{\text{g/cm}^2}$, $b = 4.4 \cdot 10^{-6} \text{ g}^{-1} \text{ cm}^2$ and $E_{\mu,n} = E_\mu/\text{MeV}$. This energy–range dependence of muons in rock is shown in Fig. 1.12.

1.1.10 Synchrotron-radiation losses

There are further energy-loss processes of charged particles like *Cherenkov radiation*, *transition radiation* and *synchrotron radiation*. Cherenkov radiation and transition radiation will be discussed in those chapters where

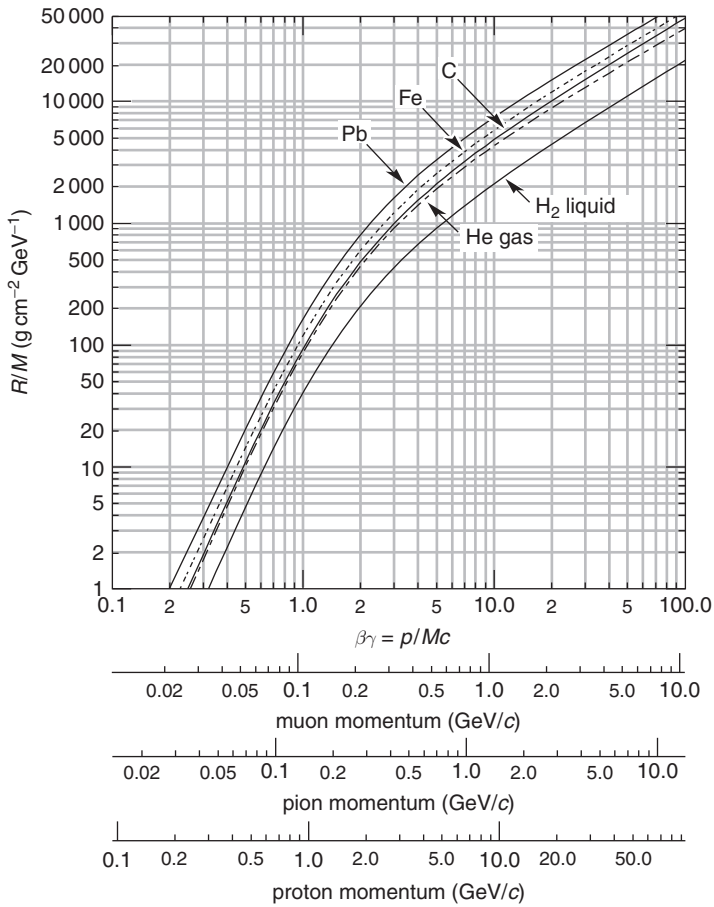


Fig. 1.11. Range of muons, pions and protons in liquid hydrogen, helium gas, carbon and lead [12].

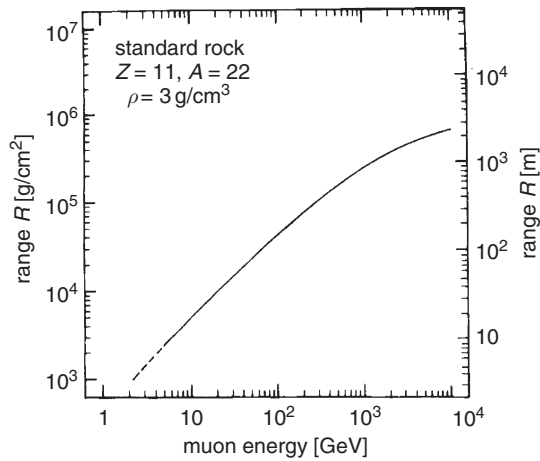


Fig. 1.12. Range of muons in rock [51].

Cherenkov detectors and transition-radiation detectors are described. Synchrotron-radiation losses are of general importance for charged-particle detection and acceleration, therefore a brief account on their essentials is given here.

Any charged particle accelerated in a straight line or on a curved path will emit electromagnetic radiation. This energy loss is particularly important for electrons deflected in a magnetic field.

The radiated power from an accelerated electron can be worked out from classical electrodynamics,

$$P = \frac{1}{4\pi\epsilon_0} \frac{2e^2}{3c^3} a^2, \quad (1.83)$$

where a is the acceleration. For the general case one has to consider relativistic effects. From

$$a = \frac{1}{m_0} \frac{dp}{d\tau} \quad (1.84)$$

and the proper time $\tau = t/\gamma$ one gets

$$a = \frac{1}{m_0} \cdot \gamma \frac{d(\gamma m_0 v)}{dt} = \gamma^2 \frac{dv}{dt} = \gamma^2 \cdot \frac{v^2}{r} \quad (1.85)$$

for an acceleration on a circle of radius r (v^2/r is the centrifugal acceleration).

This gives [40, 52]

$$P = \frac{1}{4\pi\epsilon_0} \frac{2e^2}{3c^3} \gamma^4 \frac{v^4}{r^2} = \frac{1}{6\pi\epsilon_0} e^2 c \frac{\gamma^4}{r^2} \quad (1.86)$$

for relativistic particles with $v \approx c$. For electrons one gets

$$P = \frac{e^2 c}{6\pi\epsilon_0} \left(\frac{E}{m_e c^2} \right)^4 \cdot \frac{1}{r^2} = 4.22 \cdot 10^3 \frac{E^4 [\text{GeV}^4]}{r^2 [\text{m}^2]} \text{ GeV/s} . \quad (1.87)$$

The energy loss per turn in a circular accelerator is

$$\Delta E = P \cdot \frac{2\pi r}{c} = \frac{e^2}{3\epsilon_0} \frac{\gamma^4}{r} = 8.85 \cdot 10^{-5} \frac{E^4 [\text{GeV}^4]}{r [\text{m}]} \text{ GeV} . \quad (1.88)$$

For the Large Electron–Positron collider LEP at CERN with a bending radius in the dipoles of 3100 m one obtains for a beam energy of 100 GeV

$$\Delta E = 2.85 \text{ GeV per turn} , \quad (1.89)$$

while for the Large Hadron Collider LHC for proton beam energies of 7 TeV in the LEP tunnel one has

$$\Delta E = 8.85 \cdot 10^{-5} \cdot \left(\frac{m_e}{m_p} \right)^4 \frac{E^4 [\text{GeV}^4]}{r [\text{m}]} \text{ GeV} = 6 \cdot 10^{-6} \text{ GeV} = 6 \text{ keV} . \quad (1.90)$$

The emitted synchrotron photons have a broad energy spectrum with a characteristic (critical) energy of

$$E_c = \frac{3c}{2r} \hbar \gamma^3 . \quad (1.91)$$

They are emitted into a forward cone with opening angle $\propto \frac{1}{\gamma}$. In particular, for electron accelerators the synchrotron-radiation loss is a severe problem for high-energy electrons. Therefore, electron accelerators for $E \gg 100 \text{ GeV}$ have to be linear instead of circular.

On the other hand, the synchrotron radiation from circular electron machines is used for other fields of physics like solid state or atomic physics, biophysics or medical physics. Here the high *brilliance* of these machines, often augmented by extra bending magnets (*undulators* and *wigglers*) provides excellent opportunities for structure analysis of a large variety of samples. Also the dynamical behaviour of fast biological processes can be investigated.

1.2 Interactions of photons

Photons are detected indirectly via interactions in the medium of the detector. In these processes charged particles are produced which are recorded through their subsequent ionisation in the sensitive volume of the detector. Interactions of photons are fundamentally different from ionisation processes of charged particles because in every photon interaction, the photon is either completely absorbed (*photoelectric effect*, *pair production*) or scattered through a relatively large angle (*Compton effect*). Since the absorption or scattering is a statistical process, it is impossible to define a range for γ rays. A photon beam is attenuated exponentially in matter according to

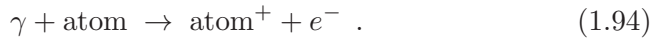
$$I = I_0 e^{-\mu x} . \quad (1.92)$$

The *mass attenuation coefficient* μ is related to the cross sections for the various interaction processes of photons according to

$$\mu = \frac{N_A}{A} \sum_i \sigma_i , \quad (1.93)$$

where σ_i is the atomic cross section for the process i , A the atomic weight and N_A the Avogadro number.

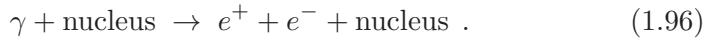
The mass attenuation coefficient (according to Eq. (1.93) given per g/cm^2) depends strongly on the photon energy. For low energies ($100 \text{ keV} \geq E_\gamma \geq \text{ionisation energy}$) the photoelectric effect dominates,



In the range of medium energies ($E_\gamma \approx 1 \text{ MeV}$) the Compton effect, which is the scattering of photons off quasi-free atomic electrons,



has the largest cross section, and at higher energies ($E_\gamma \gg 1 \text{ MeV}$) the cross section for pair production dominates,



The length x in Eq. (1.92) is an area density with the unit g/cm^2 . If the length is measured in cm , the mass attenuation coefficient μ must be divided by the density ρ of the material.

1.2.1 Photoelectric effect

Atomic electrons can absorb the energy of a photon completely, while – because of momentum conservation – this is not possible for free electrons. The absorption of a photon by an atomic electron requires a third collision partner which in this case is the atomic nucleus. The cross section for absorption of a photon of energy E_γ in the K shell is particularly large ($\approx 80\%$ of the total cross section), because of the proximity of the third collision partner, the atomic nucleus, which takes the recoil momentum. The total photoelectric cross section in the non-relativistic range away from the absorption edges is given in the non-relativistic *Born approximation* by [53]

$$\sigma_{\text{photo}}^{\text{K}} = \left(\frac{32}{\varepsilon^7} \right)^{1/2} \alpha^4 \cdot Z^5 \cdot \sigma_{\text{Th}}^e \{ \text{cm}^2/\text{atom} \} , \quad (1.97)$$

where $\varepsilon = E_\gamma/m_e c^2$ is the reduced photon energy and $\sigma_{\text{Th}}^e = \frac{8}{3} \pi r_e^2 = 6.65 \cdot 10^{-25} \text{ cm}^2$ is the *Thomson cross section* for elastic scattering of

photons on electrons. Close to the absorption edges, the energy dependence of the cross section is modified by a function $f(E_\gamma, E_\gamma^{\text{edge}})$. For higher energies ($\varepsilon \gg 1$) the energy dependence of the cross section for the photoelectric effect is much less pronounced,

$$\sigma_{\text{photo}}^{\text{K}} = 4\pi r_e^2 Z^5 \alpha^4 \cdot \frac{1}{\varepsilon} . \quad (1.98)$$

In Eqs. (1.97) and (1.98) the Z dependence of the cross section is approximated by Z^5 . This indicates that the photon does not interact with an isolated atomic electron. Z -dependent corrections, however, cause σ_{photo} to be a more complicated function of Z . In the energy range between $0.1 \text{ MeV} \leq E_\gamma \leq 5 \text{ MeV}$ the exponent of Z varies between 4 and 5.

As a consequence of the photoelectric effect in an inner shell (e.g. of the K shell) the following secondary effects may occur. If the free place, e.g. in the K shell, is filled by an electron from a higher shell, the energy difference between those two shells can be liberated in the form of X rays of characteristic energy. The energy of characteristic X rays is given by *Moseley's law*,

$$E = Ry (Z - 1)^2 \left(\frac{1}{n^2} - \frac{1}{m^2} \right) , \quad (1.99)$$

where Ry ($= 13.6 \text{ eV}$) is *Rydberg's constant* and n and m are the principal quantum numbers characterising the atomic shells. For a level transition from the L shell ($m = 2$) to the K shell ($n = 1$) one gets

$$E(\text{K}_\alpha) = \frac{3}{4} Ry (Z - 1)^2 . \quad (1.100)$$

However, this energy difference can also be transferred to an electron of the *same* atom. If this energy is larger than the binding energy of the shell in question, a further electron can leave the atom (*Auger effect*, *Auger electron*). The energy of these Auger electrons is usually quite small compared to the energy of the primary photoelectrons.

If the photoionisation occurs in the K shell (binding energy B_{K}), and if the hole in the K shell is filled up by an electron from the L shell (binding energy B_{L}), the excitation energy of the atom ($B_{\text{K}} - B_{\text{L}}$) can be transferred to an L electron. If $B_{\text{K}} - B_{\text{L}} > B_{\text{L}}$, the L electron can leave the atomic shell with an energy $B_{\text{K}} - 2B_{\text{L}}$ as an Auger electron.

1.2.2 Compton effect

The Compton effect is the scattering of photons off quasi-free atomic electrons. In the treatment of this interaction process, the binding energy of

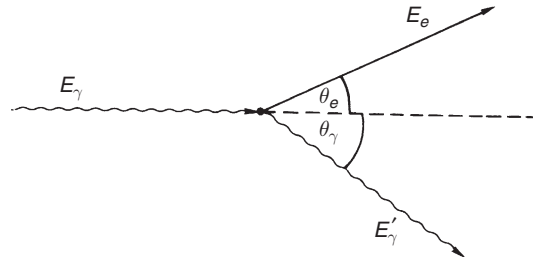


Fig. 1.13. Definition of kinematic variables in Compton scattering.

the atomic electrons is neglected. The differential probability of Compton scattering $\phi_c(E_\gamma, E'_\gamma) dE'_\gamma$ for $m_e c^2/2 < E'_\gamma < E_\gamma$ is given by the Klein–Nishina formula

$$\phi_c(E_\gamma, E'_\gamma) dE'_\gamma = \pi r_e^2 \frac{N_A Z}{A} \frac{m_e c^2}{E_\gamma} \frac{dE'_\gamma}{E'_\gamma} \left[1 + \left(\frac{E'_\gamma}{E_\gamma} \right)^2 - \frac{E'_\gamma}{E_\gamma} \sin^2 \theta_\gamma \right], \quad (1.101)$$

where θ_γ is the scattering angle of the photon in the laboratory system (see Fig. 1.13) and E_γ, E'_γ are the energies of the incident and scattered photon [54, 55]. The total cross section for Compton scattering per electron is given by [55]

$$\begin{aligned} \sigma_c^e = 2\pi r_e^2 \left[\left(\frac{1 + \varepsilon}{\varepsilon^2} \right) \left\{ \frac{2(1 + \varepsilon)}{1 + 2\varepsilon} - \frac{1}{\varepsilon} \ln(1 + 2\varepsilon) \right\} + \frac{1}{2\varepsilon} \ln(1 + 2\varepsilon) \right. \\ \left. - \frac{1 + 3\varepsilon}{(1 + 2\varepsilon)^2} \right] \{ \text{cm}^2/\text{electron} \}, \end{aligned} \quad (1.102)$$

where

$$\varepsilon = \frac{E_\gamma}{m_e c^2}. \quad (1.103)$$

The angular and energy distributions of Compton electrons are discussed in great detail in R.D. Evans [56] and G. Hertz [48]. For the energy spectrum of Compton electrons one gets

$$\frac{d\sigma_c^e}{dE_{\text{kin}}} = \frac{d\sigma_c^e}{d\Omega} \frac{2\pi}{\varepsilon^2 m_e c^2} \left[\frac{(1 + \varepsilon)^2 - \varepsilon^2 \cos^2 \theta_e}{(1 + \varepsilon)^2 - \varepsilon(2 + \varepsilon) \cos^2 \theta_e} \right]^2, \quad (1.104)$$

where

$$\frac{d\sigma_c^e}{d\Omega} = \frac{r_e^2}{2} \left(\frac{E'_\gamma}{E_\gamma} \right)^2 \left[\frac{E_\gamma}{E'_\gamma} - \frac{E'_\gamma}{E_\gamma} - \sin^2 \theta_\gamma \right]. \quad (1.105)$$

For Compton scattering off atoms the cross section is increased by the factor Z , because there are exactly Z electrons as possible scattering partners in an atom; consequently $\sigma_c^{\text{atomic}} = Z \cdot \sigma_c^e$.

At high energies the energy dependence of the Compton-scattering cross section can be approximated by [57]

$$\sigma_c^e \propto \frac{\ln \varepsilon}{\varepsilon} . \quad (1.106)$$

The ratio of scattered to incident photon energy is given by

$$\frac{E'_\gamma}{E_\gamma} = \frac{1}{1 + \varepsilon(1 - \cos \theta_\gamma)} . \quad (1.107)$$

For *backscattering* ($\theta_\gamma = \pi$) the energy transfer to the electron reaches a maximum value, leading to a ratio of scattered to incident photon energy of

$$\frac{E'_\gamma}{E_\gamma} = \frac{1}{1 + 2\varepsilon} . \quad (1.108)$$

The scattering angle of the electron with respect to the direction of the incident photon can be obtained from (see Problem 1.5)

$$\cot \theta_e = (1 + \varepsilon) \tan \frac{\theta_\gamma}{2} . \quad (1.109)$$

Because of momentum conservation the scattering angle of the electron, θ_e , can never exceed $\pi/2$.

In Compton-scattering processes only a fraction of the photon energy is transferred to the electron. Therefore, one defines an energy scattering cross section

$$\sigma_{\text{cs}} = \frac{E'_\gamma}{E_\gamma} \cdot \sigma_c^e \quad (1.110)$$

and subsequently an energy-absorption cross section

$$\sigma_{\text{ca}} = \sigma_c^e - \sigma_{\text{cs}} . \quad (1.111)$$

The latter is relevant for absorption processes and is related to the probability that an energy $E_{\text{kin}} = E_\gamma - E'_\gamma$ is transferred to the target electron.

In passing, it should be mentioned that in addition to the normal Compton scattering of photons on target electrons at rest, *inverse Compton scattering* also exists. In this case, an energetic electron collides with a low-energy photon and transfers a fraction of its kinetic energy to the

photon which is blueshifted to higher frequencies. This inverse Compton-scattering process plays an important rôle, e.g. in astrophysics. Starlight photons (eV range) can be shifted in this way by collisions with energetic electrons into the X-ray (keV) or gamma (MeV) range. Laser photons backscattered from high-energy electron beams also provide energetic γ beams which are used in accelerator experiments [58].

Naturally, Compton scattering does not only occur with electrons, but also for other charged particles. For the measurement of photons in particle detectors, however, Compton scattering off atomic electrons is of special importance.

1.2.3 Pair production

The production of electron–positron pairs in the Coulomb field of a nucleus is only possible if the photon energy exceeds a certain threshold. This threshold energy is given by the rest masses of two electrons plus the recoil energy which is transferred to the nucleus. From energy and momentum conservation, this threshold energy can be calculated to be

$$E_\gamma \geq 2m_e c^2 + 2 \frac{m_e^2}{m_{\text{nucleus}}} c^2 . \quad (1.112)$$

Since $m_{\text{nucleus}} \gg m_e$, the effective threshold can be approximated by

$$E_\gamma \geq 2m_e c^2 . \quad (1.113)$$

If, however, the electron–positron pair production proceeds in the Coulomb field of an electron, the threshold energy is

$$E_\gamma \geq 4m_e c^2 . \quad (1.114)$$

Electron–positron pair production in the Coulomb field of an electron is, however, strongly suppressed compared to pair production in the Coulomb field of the nucleus.

In the case that the nuclear charge is not screened by atomic electrons, (for low energies the photon must come relatively close to the nucleus to make pair production probable, which means that the photon sees only the ‘naked’ nucleus),

$$1 \ll \varepsilon < \frac{1}{\alpha Z^{1/3}} , \quad (1.115)$$

the pair-production cross section is given by [1]

$$\sigma_{\text{pair}} = 4\alpha r_e^2 Z^2 \left(\frac{7}{9} \ln 2\varepsilon - \frac{109}{54} \right) \{ \text{cm}^2/\text{atom} \} ; \quad (1.116)$$

for complete screening of the nuclear charge, however, ($\varepsilon \gg \frac{1}{\alpha Z^{1/3}}$) [1]

$$\sigma_{\text{pair}} = 4\alpha r_e^2 Z^2 \left(\frac{7}{9} \ln \frac{183}{Z^{1/3}} - \frac{1}{54} \right) \{ \text{cm}^2/\text{atom} \} . \quad (1.117)$$

(At high energies pair production can also proceed at relatively large impact parameters of the photon with a respect to the nucleus. But in this case the screening of the nuclear charge by the atomic electrons must be taken into account.)

For large photon energies, the pair-production cross section approaches an energy-independent value which is given by Eq. (1.117). Neglecting the small term $\frac{1}{54}$ in the bracket of this equation, this asymptotic value is given by

$$\sigma_{\text{pair}} \approx \frac{7}{9} 4\alpha r_e^2 Z^2 \ln \frac{183}{Z^{1/3}} \approx \frac{7}{9} \cdot \frac{A}{N_A} \cdot \frac{1}{X_0} , \quad (1.118)$$

see Eq. (1.51).

The partition of the energy between the produced electrons and positrons is uniform at low and medium energies and becomes slightly asymmetric at large energies. The differential cross section for the creation of a positron of total energy between E_+ and $E_+ + dE_+$ with an electron of total energy E_- is given by [53]

$$\frac{d\sigma_{\text{pair}}}{dE_+} = \frac{\alpha r_e^2}{E_\gamma - 2m_e c^2} \cdot Z^2 \cdot f(\varepsilon, Z) \{ \text{cm}^2/(\text{MeV} \cdot \text{atom}) \} . \quad (1.119)$$

$f(\varepsilon, Z)$ is a dimensionless, non-trivial function of ε and Z . The trivial Z^2 dependence of the cross section is, of course, already considered in a factor separated from $f(\varepsilon, Z)$. Therefore, $f(\varepsilon, Z)$ depends only weakly (logarithmically) on the atomic number of the absorber, see Eq. (1.117). $f(\varepsilon, Z)$ varies with Z only by few per cent [14]. The dependence of this function on the *energy-partition parameter*

$$x = \frac{E_+ - m_e c^2}{E_\gamma - 2m_e c^2} = \frac{E_+^{\text{kin}}}{E_{\text{pair}}^{\text{kin}}} \quad (1.120)$$

for average Z values is shown in Fig. 1.14 for various parameters ε [14, 59, 60]. The curves shown in Fig. 1.14 do not just include the pair production on the nucleus, but also the pair-production probability on atomic electrons ($\propto Z$), so that the Z^2 dependence of the pair-production cross section, Eq. (1.119), is modified to $Z(Z+1)$ in a similar way as was argued when the electron-bremsstrahlung process was presented, see Eq. (1.58). The angular distribution of the produced electrons is quite narrow with a characteristic opening angle of $\Theta \approx m_e c^2 / E_\gamma$.

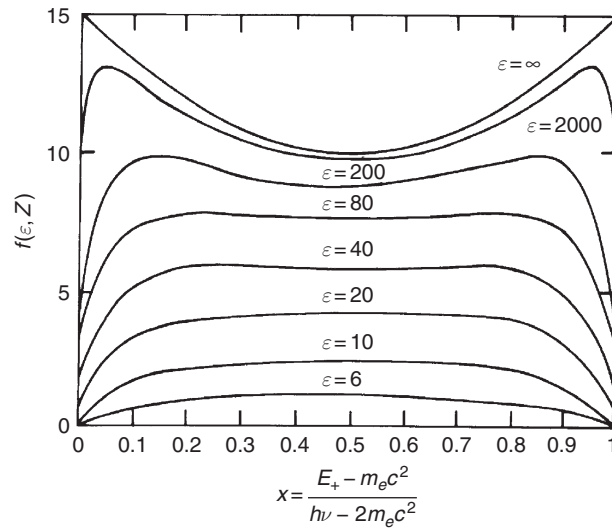


Fig. 1.14. Form of the energy-partition function $f(\varepsilon, Z, x)$ with $\varepsilon = E_\gamma/m_e c^2$ as parameter. The total pair-production cross section is given by the area under the corresponding curve in units of $Z(Z+1)\alpha r_e^2$ [14, 59, 60].

1.2.4 Total photon absorption cross section

The total mass attenuation coefficient, which is related to the cross sections according to Eq. (1.93), is shown in Figs. 1.15–1.18 for the absorbers water, air, aluminium and lead [48, 56, 61, 62].

Since Compton scattering plays a special rôle for photon interactions, because only part of the photon energy is transferred to the target electron, one has to distinguish between the *mass attenuation coefficient* and the *mass absorption coefficient*. The mass attenuation coefficient μ_{cs} is related to the Compton-energy scattering cross section σ_{cs} , see Eq. (1.110), according to Eq. (1.93). Correspondingly, the mass absorption coefficient μ_{ca} is calculated from the energy absorption cross section σ_{ca} , Eq. (1.111) and Eq. (1.93). For various absorbers the Compton-scattering cross sections, or absorption coefficients shown in Figs. 1.15–1.18, have been multiplied by the atomic number of the absorber, since the Compton-scattering cross section, Eq. (1.102), given by the Klein–Nishina formula is valid per electron, but in this case, the atomic cross sections are required.

Ranges in which the individual photon interaction processes dominate, are plotted in Fig. 1.19 as a function of the photon energy and the atomic number of the absorber [14, 50, 53].

Further interactions of photons (photonuclear interactions, *photon–photon scattering*, etc.) are governed by extremely low cross sections.

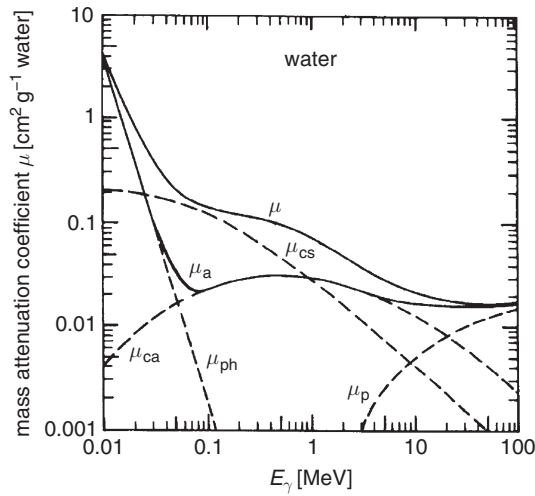


Fig. 1.15. Energy dependence of the mass attenuation coefficient μ and mass absorption coefficient μ_a for photons in water [48, 56, 61, 62]. μ_{ph} describes the photoelectric effect, μ_{cs} the Compton scattering, μ_{ca} the Compton absorption and μ_p the pair production. μ_a is the total mass absorption coefficient ($\mu_a = \mu_{ph} + \mu_p + \mu_{ca}$) and μ is the total mass attenuation coefficient ($\mu = \mu_{ph} + \mu_p + \mu_c$, where $\mu_c = \mu_{cs} + \mu_{ca}$).

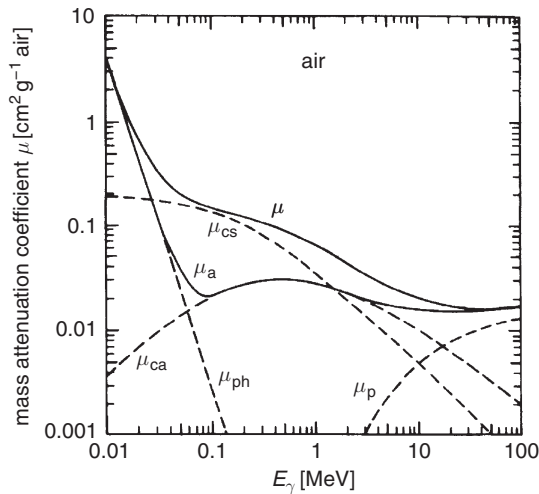


Fig. 1.16. Energy dependence of the mass attenuation coefficient μ and mass absorption coefficient μ_a for photons in air [48, 56, 61, 62].

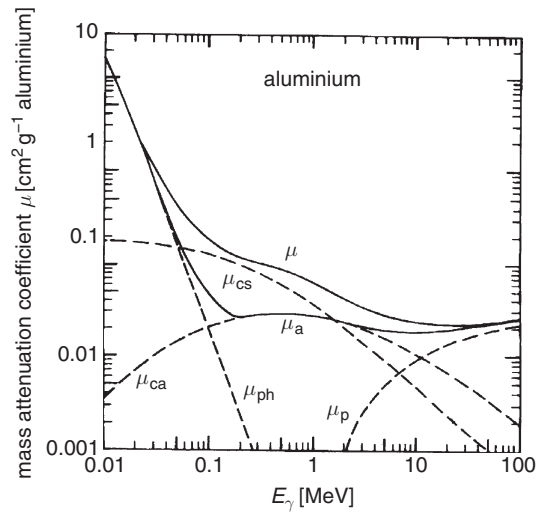


Fig. 1.17. Energy dependence of the mass attenuation coefficient μ and mass absorption coefficient μ_a for photons in aluminium [48, 56, 61, 62].

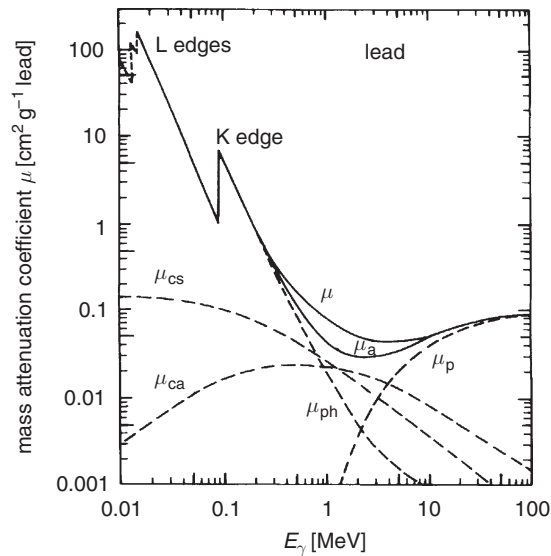


Fig. 1.18. Energy dependence of the mass attenuation coefficient μ and mass absorption coefficient μ_a for photons in lead [48, 56, 61, 62].

Therefore, these processes are of little importance for the detection of photons. However, these processes are of large interest in elementary particle physics and particle astrophysics.

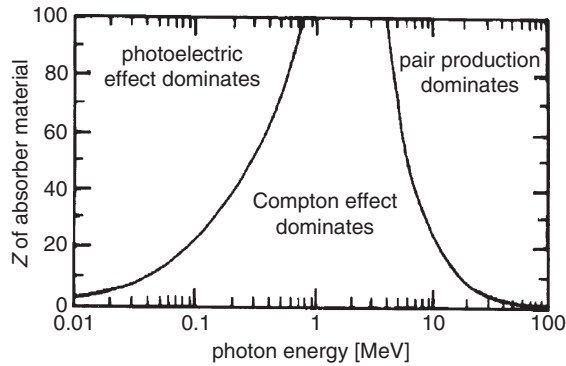


Fig. 1.19. Ranges in which the photoelectric effect, Compton effect and pair production dominate as a function of the photon energy and the target charge number Z [14, 50, 53].

1.3 Strong interactions of hadrons

Apart from the electromagnetic interactions of charged particles strong interactions may also play a rôle for particle detection. In the following we will sketch the strong interactions of hadrons.

In this case, we are dealing mostly with inelastic processes, where secondary strongly interacting particles are produced in the collision. The total cross section for proton–proton scattering can be approximated by a constant value of 50 mb ($1 \text{ mb} = 10^{-27} \text{ cm}^2$) for energies ranging from 2 GeV to 100 TeV. Both the elastic and inelastic part of the cross section show a rather strong energy dependence at low energies [12, 63],

$$\sigma_{\text{total}} = \sigma_{\text{elastic}} + \sigma_{\text{inel}} . \quad (1.121)$$

The specific quantity that characterises the inelastic processes is the average *interaction length* λ_{I} , which describes the absorption of hadrons in matter according to

$$N = N_0 e^{-x/\lambda_{\text{I}}} . \quad (1.122)$$

The value of λ_{I} can be calculated from the inelastic part of the hadronic cross section as follows:

$$\lambda_{\text{I}} = \frac{A}{N_{\text{A}} \cdot \rho \cdot \sigma_{\text{inel}}} . \quad (1.123)$$

If A is given in g/mol, N_{A} in mol^{-1} , ρ in g/cm^3 and the cross section in cm^2 , then λ_{I} has the unit cm. The area density corresponding to λ_{I} {cm}

Table 1.5. Total and inelastic cross sections as well as collision and interaction lengths for various materials derived from the corresponding cross sections [10–12]

Material	Z	A	σ_{total} [barn]	σ_{inel} [barn]	$\lambda_{\text{T}} \cdot \rho$ [g/cm ²]	$\lambda_{\text{I}} \cdot \rho$ [g/cm ²]
Hydrogen	1	1.01	0.0387	0.033	43.3	50.8
Helium	2	4.0	0.133	0.102	49.9	65.1
Beryllium	4	9.01	0.268	0.199	55.8	75.2
Carbon	6	12.01	0.331	0.231	60.2	86.3
Nitrogen	7	14.01	0.379	0.265	61.4	87.8
Oxygen	8	16.0	0.420	0.292	63.2	91.0
Aluminium	13	26.98	0.634	0.421	70.6	106.4
Silicon	14	28.09	0.660	0.440	70.6	106.0
Iron	26	55.85	1.120	0.703	82.8	131.9
Copper	29	63.55	1.232	0.782	85.6	134.9
Tungsten	74	183.85	2.767	1.65	110.3	185
Lead	82	207.19	2.960	1.77	116.2	194
Uranium	92	238.03	3.378	1.98	117.0	199

would be $\lambda_{\text{I}} \cdot \rho$ {g/cm²}. The collision length λ_{T} is related to the total cross section σ_{total} according to

$$\lambda_{\text{T}} = \frac{A}{N_{\text{A}} \cdot \rho \cdot \sigma_{\text{total}}} . \quad (1.124)$$

Since $\sigma_{\text{total}} > \sigma_{\text{inel}}$, it follows that $\lambda_{\text{T}} < \lambda_{\text{I}}$.

The interaction and collision lengths for various materials are given in Table 1.5 [10–12].

Strictly speaking, the hadronic cross sections depend on the energy and vary somewhat for different strongly interacting particles. For the calculation of the interaction and collision lengths, however, the cross sections σ_{inel} and σ_{total} have been assumed to be energy independent and independent of the particle species (protons, pions, kaons, etc.).

For target materials with $Z \geq 6$ the interaction and collision lengths, respectively, are much larger than the radiation lengths X_0 (compare Table 1.4).

The definitions for λ_{I} and λ_{T} are not uniform in the literature.

The cross sections can be used to calculate the probabilities for interactions in a simple manner. If σ_{N} is the nuclear-interaction cross section

(i.e. per nucleon), the corresponding probability for an interaction per g/cm^2 is calculated to be

$$\phi\{\text{g}^{-1} \text{cm}^2\} = \sigma_{\text{N}} \cdot N_{\text{A}} [\text{mol}^{-1}]/\text{g} , \quad (1.125)$$

where N_{A} is Avogadro's number. In the case that the atomic cross section σ_{A} is given, it follows that

$$\phi\{\text{g}^{-1} \text{cm}^2\} = \sigma_{\text{A}} \cdot \frac{N_{\text{A}}}{A} , \quad (1.126)$$

where A is the atomic weight.

1.4 Drift and diffusion in gases[‡]

Electrons and ions, produced in an ionisation process, quickly lose their energy by multiple collisions with atoms and molecules of a gas. They approach a thermal energy distribution, corresponding to the temperature of the gas.

Their average energy at room temperature is

$$\varepsilon = \frac{3}{2}kT = 40 \text{ meV} , \quad (1.127)$$

where k is the Boltzmann constant and T the temperature in Kelvin. They follow a Maxwell–Boltzmann distribution of energies like

$$F(\varepsilon) = \text{const} \cdot \sqrt{\varepsilon} \cdot e^{-\varepsilon/kT} . \quad (1.128)$$

The locally produced ionisation diffuses by multiple collisions corresponding to a Gaussian distribution

$$\frac{dN}{N} = \frac{1}{\sqrt{4\pi Dt}} \exp\left(-\frac{x^2}{4Dt}\right) dx , \quad (1.129)$$

where $\frac{dN}{N}$ is the fraction of the charge which is found in the length element dx at a distance x after a time t . D is the diffusion coefficient. For linear or volume diffusion, respectively, one obtains

$$\sigma_x = \sqrt{2Dt} , \quad (1.130)$$

$$\sigma_{\text{vol}} = \sqrt{3} \cdot \sigma_x = \sqrt{6Dt} . \quad (1.131)$$

[‡] Extensive literature to these processes is given in [2, 3, 12, 31, 32, 64–70].

Table 1.6. Average mean free path λ_{ion} , diffusion constant D_{ion} and mobilities μ_{ion} of ions in some gases for standard pressure and temperature [32, 71]

Gas	λ_{ion} [cm]	D_{ion} [cm ² /s]	μ_{ion} [$\frac{\text{cm/s}}{\text{V/cm}}$]
H ₂	$1.8 \cdot 10^{-5}$	0.34	13.0
He	$2.8 \cdot 10^{-5}$	0.26	10.2
Ar	$1.0 \cdot 10^{-5}$	0.04	1.7
O ₂	$1.0 \cdot 10^{-5}$	0.06	2.2

The average mean free path in the diffusion process is

$$\lambda = \frac{1}{N\sigma(\varepsilon)} , \quad (1.132)$$

where $\sigma(\varepsilon)$ is the energy-dependent collision cross section, and $N = \frac{N_A}{A} \rho$ the number of molecules per unit volume. For noble gases one has $N = 2.69 \cdot 10^{19}$ molecules/cm³ at standard pressure and temperature.

If the charge carriers are exposed to an electric field, an ordered drift along the field will be superimposed over the statistically disordered diffusion. A drift velocity can be defined according to

$$\vec{v}_{\text{drift}} = \mu(E) \cdot \vec{E} \cdot \frac{p_0}{p} , \quad (1.133)$$

where

$\mu(E)$ – energy-dependent charge-carrier mobility,

\vec{E} – electric field strength, and

p/p_0 – pressure normalised to standard pressure.

The statistically disordered transverse diffusion, however, is not influenced by the electric field.

The drift of free charge carriers in an electric field requires, however, that electrons and ions do not recombine and that they are also not attached to atoms or molecules of the medium in which the drift proceeds.

Table 1.6 contains numerical values for the average mean free path, the diffusion constant and the mobilities of ions [32, 71]. The mobility of ions does not depend on the field strength. It varies inversely proportional to the pressure, i.e. $\mu \cdot p \approx \text{const}$ [72, 73].

The corresponding quantity for electrons strongly depends on the energy of the electrons and thereby on the field strength. The mobilities

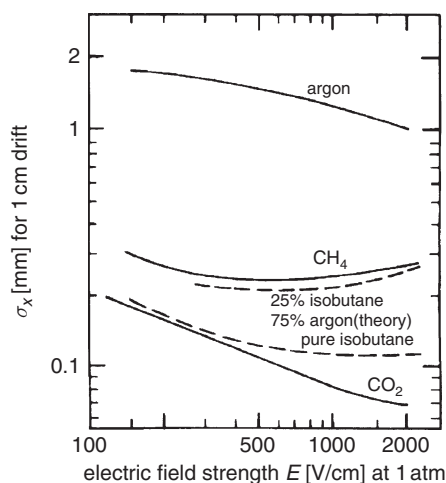


Fig. 1.20. Dependence of the root-mean-square deviation of an originally localised electron cloud after a drift of 1 cm in various gases [32, 74].

of electrons in gases exceed those of ions by approximately three orders of magnitude.

Figure 1.20 shows the root-mean-square deviation of an originally localised electron cloud for a drift of 1 cm [32, 74]. The width of the electron cloud $\sigma_x = \sqrt{2Dt}$ per 1 cm drift varies significantly with the field strength and shows characteristic dependences on the gas. For a gas mixture of argon (75%) and isobutane (25%) values around $\sigma_x \approx 200 \mu\text{m}$ are measured, which limit the spatial resolution of drift chambers. In principle, one has to distinguish between the *longitudinal diffusion* in the direction of the field and a *transverse diffusion* perpendicular to the electric field. The spatial resolution of drift chambers, however, is limited primarily by the longitudinal diffusion.

In a simple theory [75] the electron *drift velocity* can be expressed by

$$\vec{v}_{\text{drift}} = \frac{e}{m} \vec{E} \tau(\vec{E}, \varepsilon), \quad (1.134)$$

where \vec{E} is the field strength and τ the time between two collisions, which in itself depends on \vec{E} . The collision cross section, and as a consequence also τ , depends strongly on the electron energy ε and passes through pronounced maxima and minima (*Ramsauer effect*). These phenomena are caused by interference effects, if the electron wavelength $\lambda = h/p$ (h – Planck’s constant, p – electron momentum) approaches molecular dimensions. Of course, the electron energy and electric field strength are correlated. Figure 1.21 shows the Ramsauer cross section for electrons in argon as a function of the electron energy [76–81].

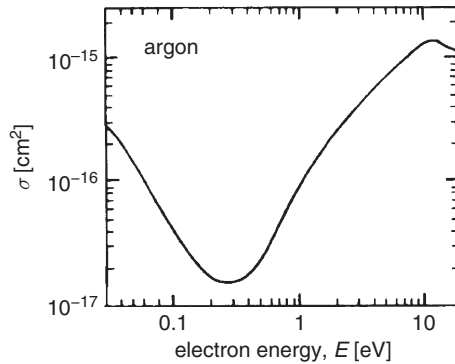


Fig. 1.21. Ramsauer cross section for electrons in argon as a function of the electron energy [76–81].

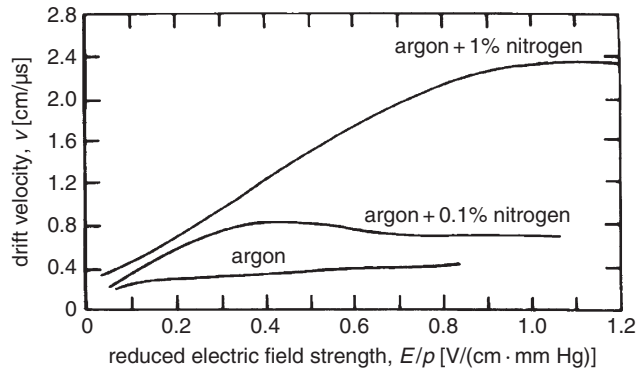


Fig. 1.22. Drift velocities of electrons in pure argon and in argon with minor additions of nitrogen [32, 76, 82, 83].

Even small contaminations of a gas can drastically modify the drift velocity (Fig. 1.22 [32, 76, 82, 83]).

Figure 1.23 shows the drift velocities for electrons in argon–methane mixtures [32, 84–86] and Fig. 1.24 those in argon–isobutane mixtures [32, 85, 87–89].

As an approximate value for high field strengths in argon–isobutane mixtures a typical value for the drift velocity of

$$v_{\text{drift}} = 5 \text{ cm}/\mu\text{s} \quad (1.135)$$

is observed. The dependence of the drift velocity on the field strength, however, may vary considerably for different gases [69, 85, 90]. Under comparable conditions the ions in a gas are slower by three orders of magnitude compared to electrons.

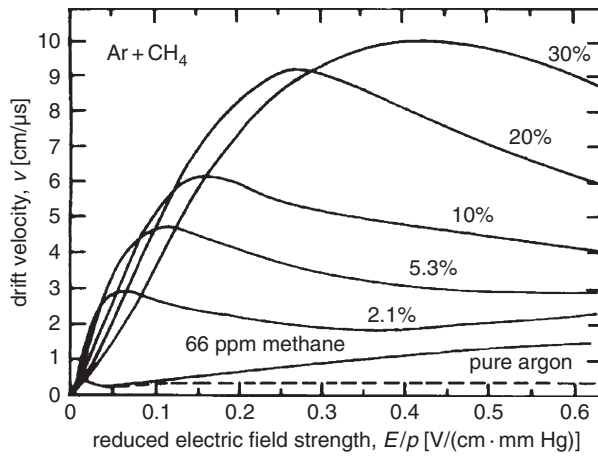


Fig. 1.23. Drift velocities for electrons in argon–methane mixtures [32, 84–86]. The percentage of methane is indicated on the curves.

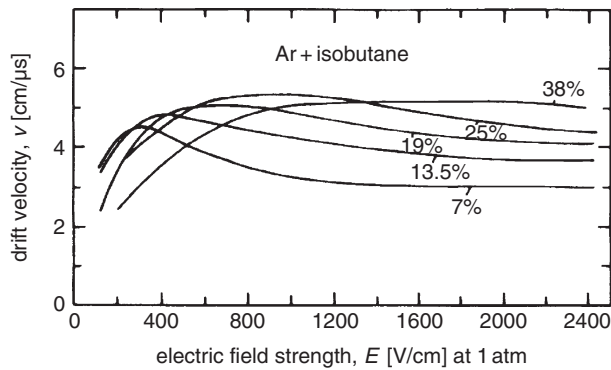


Fig. 1.24. Drift velocities for electrons in argon–isobutane mixtures [32, 85, 87–89]. The percentage of isobutane is indicated on the curves.

The drift velocity and, in general, the drift properties of electrons in gases are strongly modified in the presence of a magnetic field. In addition to the electric force, now the *Lorentz force* also acts on the charge carriers and forces the charge carriers into circular or spiral orbits.

The equation of motion for the free charge carriers reads

$$m\ddot{\vec{x}} = q\vec{E} + q \cdot \vec{v} \times \vec{B} + m\vec{A}(t) , \quad (1.136)$$

where $m\vec{A}(t)$ is a time-dependent stochastic force, which has its origin in collisions with gas molecules. If one assumes that the time average of the product $m \cdot \vec{A}(t)$ can be represented by a velocity-proportional friction

force $-m\vec{v}/\tau$, where τ is the average time between two collisions, the drift velocity can be derived from Eq. (1.136) [31] to be

$$\vec{v}_{\text{drift}} = \frac{\mu}{1 + \omega^2\tau^2} \left(\vec{E} + \frac{\vec{E} \times \vec{B}}{B} \omega\tau + \frac{(\vec{E} \cdot \vec{B}) \cdot \vec{B}}{B^2} \omega^2\tau^2 \right), \quad (1.137)$$

if one assumes that for a constant electric field a drift with constant velocity is approached, i.e., $\dot{\vec{v}}_{\text{drift}} = 0$. In Eq. (1.137)

$$\begin{aligned} \mu &= e \cdot \tau/m \text{ is the mobility of the charge carriers, and} \\ \omega &= e \cdot B/m \text{ is the cyclotron frequency (from } mr\omega^2 = evB). \end{aligned}$$

In the presence of electric and magnetic fields the drift velocity has components in the direction of \vec{E} , of \vec{B} , and perpendicular to \vec{E} and \vec{B} [91], see also Eq. (1.137). If $\vec{E} \perp \vec{B}$, the drift velocity \vec{v}_{drift} along a line forming an angle α with the electric field can be derived from Eq. (1.137) to be

$$|\vec{v}_{\text{drift}}| = \frac{\mu E}{\sqrt{1 + \omega^2\tau^2}}. \quad (1.138)$$

The angle between the drift velocity \vec{v}_{drift} and \vec{E} (*Lorentz angle*) can be calculated from Eq. (1.137) under the assumption of $\vec{E} \perp \vec{B}$,

$$\tan \alpha = \omega\tau; \quad (1.139)$$

if τ is taken from Eq. (1.134), it follows that

$$\tan \alpha = v_{\text{drift}} \cdot \frac{B}{E}. \quad (1.140)$$

This result may also be derived if the ratio of the acting Lorentz force $e\vec{v} \times \vec{B}$ (with $\vec{v} \perp \vec{B}$) to the electric force $e\vec{E}$ is considered.

For $E = 500 \text{ V/cm}$ and a drift velocity in the electric field of $v_{\text{drift}} = 3.5 \text{ cm}/\mu\text{s}$, a drift velocity in a combined electric and magnetic field ($\vec{E} \perp \vec{B}$) is obtained from Eq. (1.138) for $B = 1.5 \text{ T}$ on the basis of these simple considerations to be

$$v(E = 500 \text{ V/cm}, B = 1.5 \text{ T}) = 2.4 \text{ cm}/\mu\text{s}; \quad (1.141)$$

correspondingly the Lorentz angle is calculated from Eq. (1.140) to be

$$\alpha = 46^\circ, \quad (1.142)$$

which is approximately consistent with the experimental findings and the results of a more exact calculation (Fig. 1.25) [32, 87].

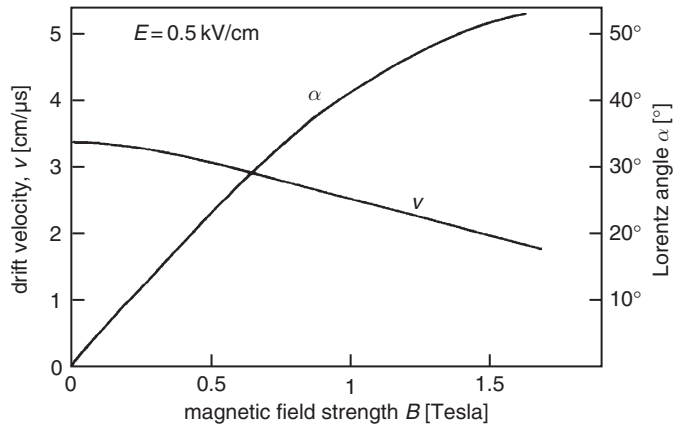


Fig. 1.25. Dependence of the electron drift velocity \vec{v}_{drift} and the Lorentz angle α on the magnetic field for low electric field strengths (500 V/cm) in a gas mixture of argon (67.2%), isobutane (30.3%) and methylal (2.5%) [32, 87].

Small admixtures of electronegative gases (e.g. oxygen) considerably modify the drift behaviour due to electron attachment. For a 1% fraction of oxygen in argon at a drift field of 1 kV/cm the average mean free path of electrons for attachment is of the order 5 cm. Small admixtures of electronegative gases will reduce the charge signal and in case of strong electronegative gases (such as chlorine) operation of a drift chamber may be even impossible.

Because of the high density the effect of impurities is even more pronounced for liquefied gases. For liquid-noble-gas chambers the oxygen concentration must stay below the ppm ($\equiv 10^{-6}$) level. ‘Warm’ liquids, like tetramethylsilane (TMS) even require to reduce the concentration of electronegative impurities to below ppb ($\equiv 10^{-9}$).

1.5 Problems

- 1.1 The range of a 100 keV electron in water is about 200 μm . Estimate its stopping time.
- 1.2 The energy loss of TeV muons in rock can be parametrised by

$$-\frac{dE}{dx} = a + bE,$$

where a stands for a parametrisation of the ionisation loss and the b term includes bremsstrahlung, direct electron-pair production and nuclear interactions ($a \approx 2 \text{ MeV}/(\text{g}/\text{cm}^2)$, $b = 4.4 \cdot 10^{-6} (\text{g}/\text{cm}^2)^{-1}$) Estimate the range of a 1 TeV muon in rock.

- 1.3** Monoenergetic electrons of 500 keV are stopped in a silicon counter. Work out the energy resolution of the semiconductor detector if a Fano factor of 0.1 at 77 K is assumed.
- 1.4** For non-relativistic particles of charge z the Bethe–Bloch formula can be approximated by

$$-\frac{dE_{\text{kin}}}{dx} = a \frac{z^2}{E_{\text{kin}}} \ln(bE_{\text{kin}}) ,$$

where a and b are material-dependent constants (different from those in Problem 1.2). Work out the energy–range relation if $\ln(bE_{\text{kin}})$ can be approximated by $(bE_{\text{kin}})^{1/4}$.

- 1.5** In *Compton telescopes* for astronomy or medical imaging one frequently needs the relation between the scattering angle of the electron and that of the photon. Work out this relation from momentum conservation in the scattering process.
- 1.6** The ionisation trail of charged particles in a gaseous detector is mostly produced by low-energy electrons. Occasionally, a larger amount of energy can be transferred to electrons (δ rays, knock-on electrons). Derive the maximum energy that a 100 GeV muon can transfer to a free electron at rest in a μe collision.
- 1.7** The production of δ rays can be described by the Bethe–Bloch formula. To good approximation the probability for δ -ray production is given by

$$\phi(E) dE = K \frac{1}{\beta^2} \frac{Z}{A} \cdot \frac{x}{E^2} dE ,$$

where

$$K = 0.154 \text{ MeV}/(\text{g}/\text{cm}^2),$$

Z, A = atomic number and mass of the target,

x = absorber thickness in g/cm^2 .

Work out the probability that a 10 GeV muon produces a δ ray of more than $E_0 = 10 \text{ MeV}$ in an 1 cm argon layer (gas at standard room temperature and pressure).

- 1.8** Relativistic particles suffer an approximately constant ionisation energy loss of about $2 \text{ MeV}/(\text{g}/\text{cm}^2)$. Work out the *depth–intensity relation* of cosmic-ray muons in rock and estimate the intensity variation if a cavity of height $\Delta h = 1 \text{ m}$ at a depth of 100 m were in the muon beam.

References

- [1] B. Rossi, *High Energy Particles*, Prentice-Hall, Englewood Cliffs (1952)
- [2] B. Sitar, G.I. Merson, V.A. Chechin & Yu.A. Budagov, *Ionization Measurements in High Energy Physics* (in Russian), Energoatomizdat, Moskau (1988)
- [3] B. Sitar, G.I. Merson, V.A. Chechin & Yu.A. Budagov, *Ionization Measurements in High Energy Physics*, Springer Tracts in Modern Physics, Vol. 124, Springer, Berlin/Heidelberg (1993)
- [4] H.A. Bethe, Theorie des Durchgangs schneller Korpuskularstrahlen durch Materie, *Ann. d. Phys.* **5** (1930) 325–400
- [5] H.A. Bethe, Bremsformel für Elektronen mit relativistischen Geschwindigkeiten, *Z. Phys.* **76** (1932) 293–9
- [6] F. Bloch, Bremsvermögen von Atomen mit mehreren Elektronen, *Z. Phys.* **81** (1933) 363–76
- [7] R.M. Sternheimer & R.F. Peierls, General Expression for the Density Effect for the Ionization Loss of Charged Particles, *Phys. Rev.* **B3** (1971) 3681–92
- [8] E.A. Uehling, Penetration of Heavy Charged Particles in Matter, *Ann. Rev. Nucl. Part. Sci.* **4** (1954) 315–50
- [9] S. Hayakawa, *Cosmic Ray Physics*, John Wiley & Sons Inc. (Wiley Interscience) (1969)
- [10] Particle Data Group, Review of Particle Properties, *Phys. Lett.* **239** (1990) 1–516
- [11] Particle Data Group, Review of Particle Properties, *Phys. Rev.* **D45** (1992) 1–574; Particle Data Group, *Phys. Rev.* **D46** (1992) 5210-0 (Errata)
- [12] Particle Data Group, Review of Particle Physics, S. Eidelman *et al.*, *Phys. Lett.* **B592 Vol. 1–4** (2004) 1–1109; W.-M. Yao *et al.*, *J. Phys.* **G33** (2006) 1–1232; <http://pdg.lbl.gov>
- [13] C. Serre, *Evaluation de la Perte D’Energie et du Parcours de Particules Chargées Traversant un Absorbant Quelconque*, CERN **67-5** (1967)
- [14] P. Marmier, *Kernphysik I*, Verlag der Fachvereine, Zürich (1977)
- [15] L. Landau, On the Energy Loss of Fast Particles by Ionization, *J. Phys. USSR* **8** (1944) 201–5
- [16] R.S. Kölbig, *Landau Distribution*, CERN Program Library G 110, CERN Program Library Section (1985)
- [17] P.V. Vavilov, Ionization Losses of High Energy Heavy Particles, *Sov. Phys. JETP* **5** (1957) 749–51
- [18] R. Werthenbach, *Elektromagnetische Wechselwirkungen von 200 GeV Myonen in einem Streamerrohr-Kalorimeter*, Diploma Thesis, University of Siegen (1987)
- [19] S. Behrends & A.C. Melissinos, *Properties of Argon–Ethane/Methane Mixtures for Use in Proportional Counters*, University of Rochester, Preprint UR-776 (1981)
- [20] J.E. Moyal, Theory of Ionization Fluctuations, *Phil. Mag.* **46** (1955), 263–80

- [21] R.K. Bock *et al.* (eds.), *Formulae and Methods in Experimental Data Evaluation*, General Glossary, Vol. 1, European Physical Society, CERN/Geneva (1984) 1–231
- [22] Y. Iga *et al.*, Energy Loss Measurements for Charged Particles and a New Approach Based on Experimental Results, *Nucl. Instr. Meth.* **213** (1983) 531–7
- [23] K. Affholderbach *et al.*, Performance of the New Small Angle Monitor for Background (SAMBA) in the ALEPH Experiment at CERN, *Nucl. Instr. Meth.* **A410** (1998) 166–75
- [24] S.I. Striganov, Ionization Straggling of High Energy Muons in Thick Absorbers, *Nucl. Instr. Meth.* **A322** (1992) 225–30
- [25] C. Grupen, Electromagnetic Interactions of High Energy Cosmic Ray Muons, *Fortschr. der Physik* **23** (1976) 127–209
- [26] U. Fano, Penetration of Photons, Alpha Particles and Mesons, *Ann. Rev. Nucl. Sci.* **13** (1963) 1–66
- [27] G. Musiol, J. Ranft, R. Reif & D. Seeliger, *Kern- und Elementarteilchenphysik*, VCH Verlagsgesellschaft, Weinheim (1988)
- [28] W. Heitler, *The Quantum Theory of Radiation*, Clarendon Press, Oxford (1954)
- [29] S.P. Møller, *Crystal Channeling or How to Build a ‘1000 Tesla Magnet’*, CERN-94-05 (1994)
- [30] D.S. Gemmell, Channeling and Related Effects in the Motion of Charged Particles through Crystals, *Rev. Mod. Phys.* **46** (1974) 129–227
- [31] K. Kleinknecht, *Detektoren für Teilchenstrahlung*, Teubner, Stuttgart (1984, 1987, 1992); *Detectors for Particle Radiation*, Cambridge University Press, Cambridge (1986)
- [32] F. Sauli, *Principles of Operation of Multiwire Proportional and Drift Chambers*, CERN-77-09 (1977) and references therein
- [33] N.I. Koschkin & M.G. Schirkewitsch, *Elementare Physik*, Hanser, München/Wien (1987)
- [34] U. Fano, Ionization Yield of Radiations. II. The Fluctuation of the Number of Ions, *Phys. Rev.* **72** (1947) 26–9
- [35] A.H. Walenta, *Review of the Physics and Technology of Charged Particle Detectors*, Preprint University of Siegen SI-83-23 (1983)
- [36] G. Lutz, *Semiconductor Radiation Detectors*, Springer, Berlin (1999)
- [37] H.A. Bethe, Molière’s Theory of Multiple Scattering, *Phys. Rev.* **89** (1953) 1256–66
- [38] C. Grupen, *Physics for Particle Detection*, Siegen University publication ed. B. Wenclawiak, S. Wilnewski (2004); Proceedings of the 10 ICFA School on Instrumentation in Elementary Particle Physics Itacuruça, Rio de Janeiro 2003 (to be published 2007); www.cbpf.br/icfa2003/
- [39] H.A. Bethe & W. Heitler, Stopping of Fast Particles and Creation of Electron Pairs, *Proc. R. Soc. Lond.* **A146** (1934) 83–112
- [40] E. Lohrmann, *Hochenergiephysik*, Teubner, Stuttgart (1978, 1981, 1986, 1992)

- [41] U. Amaldi, Fluctuations in Calorimetric Measurements, *Phys. Scripta* **23** (1981) 409–24
- [42] W. Lohmann, R. Kopp & R. Voss, *Energy Loss of Muons in the Energy Range 1 – 10.000 GeV*, CERN-85-03 (1985)
- [43] M.J. Tannenbaum, *Simple Formulas for the Energy Loss of Ultrarelativistic Muons by Direct Pair Production*, Brookhaven National Laboratory, BNL-44554 (1990)
- [44] W.K. Sakumoto *et al.*, Measurement of TeV Muon Energy Loss in Iron, University of Rochester UR-1209 (1991); *Phys. Rev.* **D45** (1992) 3042–50
- [45] K. Mitsui, Muon Energy Loss Distribution and its Applications to the Muon Energy Determination, *Phys. Rev.* **D45** (1992) 3051–60
- [46] Lev I. Dorman, *Cosmic Rays in the Earth's Atmosphere and Underground*, Kluwer Academic Publishers, Dordrecht (2004)
- [47] R. Baumgart *et al.*, Interaction of 200 GeV Muons in an Electromagnetic Streamer Tube Calorimeter, *Nucl. Instr. Meth.* **A258** (1987) 51–7
- [48] G. Hertz, *Lehrbuch der Kernphysik*, Bd. 1, Teubner, Leipzig (1966)
- [49] J.S. Marshall & A.G. Ward, Absorption Curves and Ranges for Homogeneous β -Rays, *Canad. J. Res.* **A15** (1937) 39–41
- [50] E. Sauter, *Grundlagen des Strahlenschutzes*, Siemens AG, Berlin/München (1971); *Grundlagen des Strahlenschutzes*, Thiemig, München (1982)
- [51] A.G. Wright, A Study of Muons Underground and Their Energy Spectrum at Sea Level, Polytechnic of North London Preprint (1974); *J. Phys.* **A7** (1974) 2085–92
- [52] R.K. Bock & A. Vasilescu, *The Particle Detector Briefbook*, Springer, Heidelberg (1998)
- [53] P. Marmier & E. Sheldon, *Physics of Nuclei and Particles*, Vol. 1, Academic Press, New York (1969)
- [54] E. Fenyves & O. Haimann, *The Physical Principles of Nuclear Radiation Measurements*, Akadémiai Kiadó, Budapest (1969)
- [55] O. Klein & Y. Nishina, Über die Streuung von Strahlung durch freie Elektronen nach der neuen relativistischen Quantenmechanik von Dirac, *Z. Phys.* **52** (1929) 853–68
- [56] R.D. Evans, *The Atomic Nucleus*, McGraw-Hill, New York (1955)
- [57] W.S.C. Williams, *Nuclear and Particle Physics*, Clarendon Press, Oxford (1991)
- [58] V. Telnov, *Photon Collider at TESLA*, hep-ex/0010033v4 (2000); *Nucl. Instr. Meth.* **A472** (2001) 43
- [59] C. Grupen & E. Hell, Lecture Notes, *Kernphysik*, University of Siegen (1983)
- [60] H.A. Bethe & J. Ashkin, Passage of Radiation through Matter, in E. Segrè (ed.), *Experimental Nucl. Phys.*, Vol. 1, John Wiley & Sons Inc. (Wiley Interscience), New York (1953) 166–201
- [61] G.W. Grodstein, *X-Ray Attenuation Coefficients from 10 keV to 100 MeV*, Circ. Natl. Bur. Stand. No. 583 (1957)
- [62] G.R. White, *X-ray Attenuation Coefficients from 10 keV to 100 MeV*, Natl. Bur. Standards (U.S.) Rept. 1003 (1952)

- [63] Particle Data Group, Review of Particle Properties, *Phys. Lett.* **B111** (1982) 1–294
- [64] P. Rice-Evans, *Spark, Streamer, Proportional and Drift Chambers*, Richelieu Press, London (1974)
- [65] A. Andronic *et al.*, Drift Velocity and Gain in Argon and Xenon Based Mixtures, *Nucl. Instr. Meth.* **A523** (2004) 302–8
- [66] P. Colas *et al.*, Electron Drift Velocity Measurements at High Electric Fields, DAPNIA-01-09 (2001) 10; *Nucl. Instr. Meth.* **A478** (2002) 215–19
- [67] V. Palladino & B. Sadoulet, *Application of the Classical Theory of Electrons in Gases to Multiwire Proportional and Drift Chambers*, LBL-3013, UC-37, TID-4500-R62 (1974)
- [68] W. Blum & L. Rolandi, *Particle Detection with Drift Chambers*, Springer Monograph XV, Berlin/New York (1993)
- [69] A. Peisert & F. Sauli, *Drift and Diffusion in Gases: A Compilation*, CERN-84-08 (1984)
- [70] L.G. Huxley & R.W. Crompton, *The Diffusion and Drift of Electrons in Gases*, John Wiley & Sons Inc. (Wiley Interscience), New York (1974)
- [71] E.W. McDaniel & E.A. Mason, *The Mobility and Diffusion of Ions in Gases*, John Wiley & Sons Inc. (Wiley Interscience), New York (1973)
- [72] M.P. Langevin, Sur la mobilité des ions dans les gaz, *C. R. Acad. Sci. Paris*, **134** (1903) 646–9; Recherches sur les gaz ionisés, *Ann. Chim. et Phys.*, **28** (1903) 233–89
- [73] L.B. Loeb, *Basis Processes of Gaseous Electronics*, University of California Press, Berkeley (1961)
- [74] V. Palladino & B. Sadoulet, Application of the Classical Theory of Electrons in Gases to Multiwire Proportional and Drift Chambers, *Nucl. Instr. Meth.* **128** (1975) 323–66
- [75] J. Townsend, *Electrons in Gases*, Hutchinson, London (1947)
- [76] S.C. Brown, *Basic Data of Plasma Physics*, MIT Press, Cambridge, MA. (1959), and John Wiley & Sons, Inc., New York (1959)
- [77] C. Ramsauer & R. Kollath, Die Winkelverteilung bei der Streuung langsamer Elektronen an Gasmolekülen, *Ann. Phys.* **401** (1931) 756–68
- [78] C. Ramsauer & R. Kollath, Über den Wirkungsquerschnitt der Edelgas-moleküle gegenüber Elektronen unterhalb 1 Volt, *Ann. Phys.* **395** (1929) 536–64
- [79] C. Ramsauer, Über den Wirkungsquerschnitt der Gasmoleküle gegenüber langsamen Elektronen, *Ann. Phys.* **64** (1921) 513–40
- [80] E. Brüche *et al.*, Über den Wirkungsquerschnitt der Edelgase Ar, Ne, He gegenüber langsamen Elektronen, *Ann. Phys.* **389** (1927) 279–91
- [81] C.E. Normand, The Absorption Coefficient for Slow Electrons in Gases, *Phys. Rev.* **35** (1930) 1217–25
- [82] L. Colli & U. Facchini, Drift Velocity of Electrons in Argon, *Rev. Sci. Instr.* **23** (1952) 39–42
- [83] J.M. Kirshner & D.S. Toffolo, Drift Velocity of Electrons in Argon and Argon Mixtures, *J. Appl. Phys.* **23** (1952) 594–8

- [84] H.W. Fulbright, Ionization Chambers in Nuclear Physics, in S. Flügge (ed.), *Handbuch der Physik*, Band **XLV**, Springer, Berlin (1958)
- [85] J. Fehlmann & G. Viertel, *Compilation of Data for Drift Chamber Operation*, ETH-Zürich-Report (1983)
- [86] W.N. English & G.C. Hanna, Grid Ionization Chamber Measurement of Electron Drift Velocities in Gas Mixtures, *Canad. J. Phys.* **31** (1953) 768–97
- [87] A. Breskin *et al.*, Recent Observations and Measurements with High-Accuracy Drift Chambers, *Nucl. Instr. Meth.* **124** (1975) 189–214
- [88] A. Breskin *et al.*, Further Results on the Operation of High-Accuracy Drift Chambers, *Nucl. Instr. Meth.* **119** (1974) 9–28
- [89] G. Charpak & F. Sauli, High-Accuracy Drift Chambers and Their Use in Strong Magnetic Fields, *Nucl. Instr. Meth.* **108** (1973) 413–26
- [90] J. Va'vra *et al.*, Measurement of Electron Drift Parameters for Helium and CF₄-Based Gases, *Nucl. Instr. Meth.* **324** (1993) 113–26
- [91] T. Kunst *et al.*, Precision Measurements of Magnetic Deflection Angles and Drift Velocities in Crossed Electric and Magnetic Fields, *Nucl. Instr. Meth.* **A423** (1993) 127–40